ZEB1 promotes chemo-immune resistance in pancreatic cancer models by downregulating chromatin acetylation of *CXCL16*

Shaobo Zhang[1,†], Yumeng Hu[1,†], Zhijun Zhou[2,3,†], Gaoyuan Lv[1], Chenze Zhang[4], Yuanyuan Guo[1], Fangxia Wang[1], Yuxin Ye[1], Haoran Qi[1], Hui Zhang[5], Wenming Wu[6], Min Li[2,3,*] and Mingyang Liu[1,*]

[1]State Key Laboratory of Molecular Oncology, National Cancer Center/National Clinical Research Center for Cancer/Cancer Hospital, Chinese Academy of Medical Sciences & Peking Union Medical College, Beijing, China

[2]Department of Medicine, the University of Oklahoma Health Sciences Center, Oklahoma City, Oklahoma, 73104, USA

[3]Department of Surgery, the University of Oklahoma Health Sciences Center, Oklahoma City, Oklahoma, 73104, USA

[4]National Key Laboratory of Efficacy and Mechanism on Chinese Medicine for Metabolic Diseases, Beijing Research Institute of Chinese Medicine, Beijing University of Chinese Medicine, Beijing, China

[5]Department of Pathology, Peking Union Medical College Hospital, Chinese Academy of Medical Sciences and Peking Union Medical College, Beijing, China

[6]Department of General Surgery, Peking Union Medical College Hospital, Chinese Academy of Medical Sciences and Peking Union Medical College, Beijing, China

[†]S Zhang, Y Hu and Z Zhou are co–first authors and contributed equally to this work.

***Correspondence to:**

Mingyang Liu, MD, PhD

State Key Laboratory of Molecular Oncology, National Cancer Center/National Clinical Research Center for Cancer/Cancer Hospital, Chinese Academy of Medical Sciences & Peking Union Medical College, Beijing, China

Email: liumy@cicams.ac.cn

Min Li, PhD

Department of Medicine, Department of Surgery

The University of Oklahoma Health Sciences Center

975 NE 10th Street, BRC 1262A, Oklahoma City, OK 73104, USA

Tel: (405) 271-6145, Fax: (405) 271-1476, Email: Min-Li@ouhsc.edu

Conflict of interest

The authors have declared that no conflict of interest exists.

Abstract

Pancreatic cancer (PC) is notoriously resistant to both chemotherapy and immunotherapy, presenting a major therapeutic challenge. Epigenetic modifications play a critical role in PC progression, yet their contribution to chemoimmunotherapy resistance remains poorly understood. Here, we identified the transcription factor ZEB1 as a critical driver of chemoimmunotherapy resistance in PC. *ZEB1* knockdown synergized with gemcitabine and anti-PD1 therapy, markedly suppressed PC growth, and prolonged survival in vivo. Single-cell and spatial transcriptomics revealed that ZEB1 ablation promoted tumor pyroptosis by recruiting and activating $GZMA^{+}CD8^{+}$ T cells in the tumor core through epigenetic upregulation of *CXCL16*. Meanwhile, ZEB1 blockade attenuates $CD44^{+}$ neutrophil-induced $CD8^{+}$ T cell exhaustion by reducing tumor-derived SPP1 secretion, which otherwise promotes exhaustion through activation of the PD-L1–PD-1 pathway. Clinically, high ZEB1 expression correlated with chemoresistance, immunosuppression, and diminished CXCL16 levels in PC patients. Importantly, the epigenetic inhibitor Mocetinostat (targeting ZEB1) potentiated chemoimmunotherapy efficacy, including anti-PD1 and CAR-T therapies, in patient-derived organoids, xenografts, and orthotopic models. Our study unveils ZEB1 as a master epigenetic regulator of chemoimmunotherapy resistance and proposes its targeting as a transformative strategy for PC treatment.

Introduction

Pancreatic cancer (PC) is one of the most lethal cancers, which was predicted to become the second leading cause of cancer-related death within this decade (1). Only a small proportion of PC patients would benefit from targeted therapy and immunotherapy (2-4). The intratumor heterogeneity, driven by the unique genomic alterations and the immunosuppressive subpopulation of immune cells and stromal cells in the tumor microenvironment, leads to immune escape and treatment resistance in PC (5-7). Combination therapies may hold the promise for improving the treatment outcomes of PC. Unfortunately, chemotherapy did not increase the effectiveness of immunotherapy in PC. Emerging evidence indicates that chemotherapy resistance has the potential to facilitate immune evasion via the upregulation of immunosuppressive molecules, such as CD47, PD-L1, and PGE_2, through metabolic or oncogenic pathway reprogramming (8, 9). It fostered an immunosuppressive microenvironment in PC (10, 11). Tumor microenvironment is critical in driving the malignant phenotypes and treatment resistance (12-16). Dissecting the mechanisms through which the reprogrammed microenvironment grants PC cells the ability to escape the cytotoxic effect of chemotherapy and immunotherapy is key to fostering potential therapeutic strategies, especially combination therapy. Cellular pyroptosis is a form of inflammatory cell death triggered by pore-forming amino-terminal fragments generated through cleavage of the Gasdermin family proteins. It is characterized by cell membrane perforation, activation of inflammasomes, and the release of pro-inflammatory cytokines such as IL-1β and IL-18. In recent years, $CD8^+$ T cells, as key effector cells of the cytotoxic immune response, have been shown to exert anti-tumor effects by inducing tumor cell pyroptosis, primarily through the release of granzyme A (GZMA) and granzyme B (GZMB). Mechanistically, GZMA induces pyroptosis in target cells by cleaving GSDMB (17), while GZMB not only activates caspase-3 in target cells (18), but also directly cleaves GSDME at the same site as caspase 3, thereby triggering pyroptosis (19). Meanwhile, gemcitabine, a nucleoside analogue, has been found to indirectly promote pyroptosis by modulating mitochondrial reactive oxygen species (ROS) and activating the caspase-3/GSDME pathway, in

addition to its direct inhibitory effects on tumor cell proliferation (20). These findings provide a potential theoretical basis for combining immunotherapy with chemotherapy.

Epigenetic modification, such as DNA and histone modification, profoundly affects the tumor immune microenvironment by dynamically modifying gene expression in the tumor microenvironment. By inhibiting DNA methylation, the suppression of immune-related genes can be reversed, leading to an increase in the number and function of tumor-infiltrating $CD8^+$ T cells, thereby restoring immune function (21). Epigenetic modification induced cancer immune evasion by decreasing tumor immunogenicity, a critical factor associated with neoantigen quality and its presentation (22, 23). Histone acetylation modulates chromatin accessibility, which plays a pivotal role in cancer immune evasion (24-29).

Histone deacetylases (HDACs) are a group of enzymes that remove the acetylation from histones. HDAC inhibition increases the sensitivity of chemotherapy and suppresses PC progression by blocking the phenotypic transformation of fibroblasts in preclinical models (30, 31). HDAC1 is identified as a marker of poor immune checkpoint blockade (ICB) response in hepatocellular carcinoma (32); its inhibition enhances $CD8^+$ T cell activity and improves immunotherapy efficacy in lung and colorectal cancers (33). However, its role in PC remains unclear. A phase 2 clinical trial showed that HDAC inhibitor had a synergistic effect when combined with anti-PD1 immunotherapy and anti-VEGF antibody in patients with proficient mismatch repair/ microsatellite stable (pMMR/MSS) colorectal cancer, who are deemed resistant to immunotherapy (34). However, whether combining immunotherapy, chemotherapy, and HDAC inhibitors would provide synergistic efficacy in PC remains to be defined. While Zinc Finger E-Box Binding Homeobox 1 (ZEB1) is known to play critical roles in chemoresistance and cellular plasticity (35, 36), its contribution to chemoimmunotherapy resistance, particularly through regulation of HDAC-associated chromatin accessibility and immune microenvironment reprogramming, remains poorly understood.

In this study, we identified that knocking down *ZEB1* substantially inhibited PC progression and increased chemo-immune response in vivo through enhancing $CD8^+$ T cells-induced pyroptosis and inhibiting crosstalk between $CD8^+$ T cells and neutrophils in PC. Treatment with Mocetinostat (an epigenetic reprogramming inhibitor of ZEB1) synergizes with gemcitabine and anti-PD1, enhancing the efficacy of chemotherapy and immunotherapy in the allograft mouse model, patient-derived organoid models, and patient-derived xenograft mouse models.

Results

ZEB1 promotes chemo-immune resistance in PC

Given that PC patients are resistant to chemoimmunotherapy, we established two human PC stable cell lines (AsPC-1-R and MIA PaCa-2-R), which are resistant to gemcitabine and inactivate $CD8^+$ T cells (Supplemental Figure 1, A-F). To investigate the underlying mechanism, we performed RNA sequencing in wild-type and chemoimmunotherapy-resistant PC cell lines. The upregulated transcription factors (TFs) in chemoimmunotherapy-resistant PC cells were merged with TFs that were upregulated in PC tissue and HDAC-interacting TFs (Supplemental Figure 1G). We identified 6 genes and finally focused on *ZEB1*, which has been reported to promote tumor progression and migration. We found that *ZEB1* was upregulated upon gemcitabine treatment as well as in gemcitabine-resistant stable cell lines (Supplemental Figure 1, H and I). Knockdown of *ZEB1* increased the sensitivity of PC to gemcitabine and activated $CD8^+$ T cells (Supplemental Figure 1, J-M).

Targeting ZEB1 activates tumor immune microenvironment (TIME) and sensitizes PC to chemoimmunotherapy

Next, we assessed the impact of *ZEB1* knockdown on chemoimmunotherapy sensitivity in vivo using an allograft PC mouse model (Supplemental Figure 1N). To investigate whether knocking down *ZEB1* synergizes with chemoimmunotherapy through TIME, control (KPC-shV) and *ZEB1*-knockdown KPC (KPC-sh*ZEB1*) cells were orthotopically inoculated into immunocompetent and immunodeficient

mice under the treatment of gemcitabine. The results showed that ZEB1 inhibition induced more dramatic tumor regression in immunocompetent mice (Figure 1, A and B). Inhibition of ZEB1 notably enhances the tumor-suppressive effect of gemcitabine and prolongs overall survival in immunocompetent mice (Figure 1, C-E and Supplemental Figure 1, O and P). Further experiments confirmed that *ZEB1* knockdown in combination with gemcitabine and anti-PD1 therapy resulted in superior tumor suppression. (Figure 1, F and G). To further investigate the function of ZEB1 on TIME, we performed single-cell RNA-sequencing (scRNA-seq) using the tumor tissue collected from mice allografted with KPC-shV or KPC-sh*ZEB1* cells treated with gemcitabine in Figure 1C (Figure 1, H and I). Compared with the control, *ZEB1* knockdown substantially increased the proportion of total T cells and $CD8^+$ T cells (Figure 1J, Supplemental Figure 1Q and Supplemental Figure 2, A and B). These findings were validated by IHC staining and flow cytometry analysis (Supplemental Figure 1, R and S). Ligand-receptor pair communication analysis revealed enhanced interaction between PC cells and T cells following *ZEB1* knockdown (Figure 1K). These findings indicated that blocking ZEB1 enhanced the chemoimmunotherapy through activating $CD8^+$ T cells in vivo.

$GZMA^+CD8^+$ T cells are enriched in *ZEB1*-knockdown tumors with gemcitabine treatment

To identify the specific functional subtype of $CD8^+$ T cells that is associated with ZEB1, $CD8^+$ T cells were further clustered into LEF1-T Naïve, LY6C2-T Naïve, GZMA-T Effector, and DSCAM-T Effector based on gene signatures (Figure 2A). Of these four subsets of $CD8^+$ T cells, the GZMA-T Effector cells ($GZMA^+CD8^+$ T cells), which constituted the largest group of cytotoxic effector T cells (cytotoxic T lymphocytes, CTLs), were increased by 3.8-fold after *ZEB1* knockdown (Figure 2, B-D). This subset was the only one that prominently featured *Gzma* (Figure 2B, and Supplemental Figure 2, C-E), whose role as a cytotoxic mediator in killing tumor cells has been widely reported (17, 37, 38). To further evaluate the role of $GZMA^+CD8^+$ T cells in PC, we performed spatial transcriptomics and multiplex immunohistochemistry (mIHC) on the same tumor tissues used for scRNA-seq. We

identified that the percentage of $GZMA^+CD8^+$ T cells was remarkably increased, especially in the core region of tumor tissues, with *ZEB1* knockdown (Figure 2, E and F). Subsequent intercellular communication analysis revealed that compared with the other three subtypes of $CD8^+$ T cells, $GZMA^+CD8^+$ T cells have the strongest interaction with tumor cells upon ZEB1 inhibition (Figure 2, G-I). These findings demonstrated that $GZMA^+CD8^+$ T cells are the main mediators of the immune response triggered by ZEB1 inhibition in PC.

ZEB1 inhibition enhances the anti-cancer response of $CD8^+$ T cells and CAR-T therapy

PC is characterized by a suppressive immune microenvironment, which severely limits CTLs response (39-41). In concordance with scRNA-seq analysis, the results of in vitro experiments illustrated that ZEB1 inhibition enhanced the recruitment and activation of $CD8^+$ T cells while reducing their apoptosis (Figure 3, A-D, and Supplemental Figure 3A). We evaluated whether the activated $CD8^+$ T cells decreased cell viability and potentiated the gemcitabine sensitivity of PC cells, and found that $CD8^+$ T cell treatment augmented gemcitabine sensitivity, which was enhanced by ZEB1 inhibition (Supplemental Figure 3, B-D). Moreover, the expression of MHC-I was upregulated in ZEB1 knockdown (KD) PC cells (Supplemental Figure 3E). MHC-I signaling analyzed by scRNA-seq data confirmed the strengthened interaction between $CD8^+$ T cells and *ZEB1* knockdown PC cells (Supplemental, Figure 3F). Besides, the CAR-T cell model was established to evaluate the tumor lysis activity both in vitro and in vivo. Under different effector-to-target (E: T) ratios, CAR-T cells that encountered *ZEB1*-KD AsPC-R cells showed elevated lysis ability, which was also validated in the model of KPC-OVA/OT1-$CD8^+$ T cell (Figure 3, E and F). Furthermore, OT1-$CD8^+$ T cells showed a dramatic anti-tumor effect in vivo when ZEB1 was knocked down in tumor tissue, highlighting the key function of ZEB1 in regulating the sensitivity of PC to CAR-T cell therapy (Figure 3, G and H). Additionally, we wondered whether the recruited $CD8^+$ T cells increased gemcitabine sensitivity by regulating the expression of genes that are associated with gemcitabine sensitivity. Equilibrative

nucleoside transporter 1 (ENT1) is a therapeutic response marker for gemcitabine. Our prior study revealed that ZEB1 induces PC gemcitabine resistance by inhibiting *ENT1* transcription (42), and thus, we wondered whether $CD8^+$ T cells could also modulate ENT1 expression. Treatment with conditioned medium (CM) of $CD8^+$ T cells upregulated ENT1 expression and enhanced Cy5-gemcitabine (Cy5-GEM) accumulation in PC cells (Figure 3I, and Supplemental Figure 3, G-I). Thus, in addition to their conventional cytotoxic effects, cytotoxic lymphocytes also upregulate ENT1 expression in PC cells, increasing their sensitivity to gemcitabine. Besides, a recent study showed that gemcitabine could foster pyroptosis by activating the Caspase 1/GSDMD pathway in PC, and pyroptosis activation by VbP, an enzymatic activator of Caspase 1, confers PC gemcitabine sensitivity (43). Meanwhile, cytotoxic lymphocytes can trigger pyroptosis in target cells (17). Accordingly, we wondered whether the recruitment of cytotoxic $CD8^+$ T cells induced by *ZEB1* knockdown could boost gemcitabine-related pyroptosis. Gene set enrichment analysis (GSEA) of differentially expressed genes in PC cells after *ZEB1* knockdown revealed pyroptosis as a statistically significant pathway (Supplemental Figure 3J). Then, we performed a classical calcium release assay to evaluate tumor pyroptosis and found that the combination of gemcitabine and CM from $CD8^+$ T cells increased calcium influx, enhancing the lethal lysis of PC cells (Figure 3J). Furthermore, knockdown of *ZEB1* acted synergistically with gemcitabine and $CD8^+$ T cells to promote pyroptosis in PC cells (Figure 3, J and K, and Supplemental Figure 3, K-L). Collectively, these results indicate that targeting ZEB1 in PC cells synergizes with gemcitabine by activating $CD8^+$ T cells, thereby enhancing anti-cancer response and cytotoxicity.

Blocking of ZEB1 activates $CD8^+$ T cells partially by inhibiting the function of neutrophils

Our scRNA-seq atlas analysis of TIME in vivo revealed that inhibition of ZEB1 not only increased the $CD8^+$ T cells population but also decreased granulocyte (neutrophil) proportion and its interaction with tumor cells (Figure 4A and Supplemental Figure 1S). The spatial transcriptomics and mIHC analyses indicated that there were fewer neutrophils infiltrated within the tumor's core region when *ZEB1* was

knocked down, aligning with our scRNA-seq findings (Figure 2F). Additionally, scRNA-seq analysis and in vitro experiments demonstrated that *ZEB1* KD inhibited neutrophil activities, including migration and polarization, thereby promoting N1-polarized neutrophil differentiation (Figure 4B-4D). Considering that neutrophils constitute a prominent immunosuppressive cell population within the TME, leading to T cell exclusion and unresponsiveness to antigen-specific stimulation (44), we intended to investigate whether *ZEB1* KD affects T cell response via neutrophils. Initially, we verified the suppressive effects of neutrophils on $CD8^+$ T cell migration in vitro (Figure 4E). To elucidate how *ZEB1* KD in tumor cells could impair the function of $CD8^+$ T cells through neutrophils, we established a coculture system with these three cell types and then collected them for subsequent analysis (Figure 4F). Assessment of $CD8^+$ T cell and neutrophil markers revealed pronounced activation of $CD8^+$ T cells and inhibition of neutrophils following *ZEB1* knockdown (Figure 4, G and H). Moreover, ZEB1 KD notably augmented the therapeutic efficacy of gemcitabine and anti-Ly6G combination therapies by decreasing the infiltration of neutrophils, while increasing the infiltration of $CD8^+$ T cells (Figure 4, I and J, and Supplemental Figure 4, A-D). To pinpoint the crucial factors mediating the interaction between PC cells and neutrophils, we analyzed intercellular communications involving ligand-receptor pairs and found that the signal of SPP1(tumor)-CD44 (neutrophil) was dramatically inhibited in the *ZEB1* KD group (Supplemental Figure 4, E-G). SPP1-CD44 is critical in neutrophil recruitment and the formation of neutrophil extracellular traps (NETs). We further confirmed that knockdown of *ZEB1* decreased SPP1 expression both in vitro and in vivo (Supplemental Figure 4, H and I). Furthermore, SPP1 recombinant protein treatment induced a dose-dependent inhibition of neutrophil cytotoxicity (Supplemental Figure S4J). And neutrophils inhibited $CD8^+$ T cells' function by downregulating *PD-L1* (Supplemental Figure 4, K and L). Taken together, targeting ZEB1 in tumor cells effectively inhibits the recruitment and polarization of neutrophils, leading to the activation of $CD8^+$ T cells and the synergistic anti-tumor effect with chemoimmunotherapy in PC.

Inhibition of ZEB1 synergizes with chemoimmunotherapy through activating *CXCL16*

To further elucidate the mechanism of ZEB1-regulated chemoimmunotherapy, we performed intercellular communication analysis using our scRNA-seq data. We identified 64 signaling pathways that were notably upregulated in ZEB1 KD tumors. Among various cytokines and chemokines in KPC cells, *CXCL16* was the most markedly upregulated upon *ZEB1* knockdown (Figure 5A and Supplemental Figure 5A). Given that CXCR6, the specific receptor for CXCL16, is reported to be highly expressed in intratumoral $CD8^+$ T cells, and that $CXCR6^+CD8^+$ T cells are critical for checkpoint blockade therapy (45-47), we hypothesized that the increased sensitivity to chemoimmunotherapy following *ZEB1* KD is attributed to the enhanced chemotaxis and activity of $CD8^+$ T cells driven by elevated *CXCL16*. We confirmed the reversed correlation between ZEB1 and CXCL16 (Supplemental Figure 5, B-E). Exogenous recombinant CXCL16 increased the migration and activation of $CD8^+$ T cells, leading to the enhanced anti-tumor effect (Supplemental Figure 5, F-K). The enhancement of tumor cell recognition and $CD8^+$ T cell activation in OT-1 T cells suggested a direct response to CXCL16 stimulation. To further delineate the role of the ZEB1/CXCL16 axis in $CD8^+$ T cell activity and the sensitivity of PC tumors to chemoimmunotherapy or T cell therapy, we investigated $CD8^+$ T cell functions. We found that *CXCL16* KD notably attenuated the migration, activation, and cytotoxicity of $CD8^+$ T cells enhanced by *ZEB1* KD (Figure 5, B-D, and Supplemental Figure 5, L-N). Notably, the therapeutic benefit of chemoimmunotherapy or T cell therapy induced by ZEB1 inhibition was notably reversed by *CXCL16* KD (Figure 5, E-H, and Figure 5, O-Q). Collectively, these results indicate that CXCL16/CXCR6 signaling, which is activated when *ZEB1* is knocked down, mediates the recruitment and activation of $CD8^+$ T cells, rendering PC tumors highly vulnerable to chemoimmunotherapy and T cell therapy.

ZEB1/HDAC1 complex suppressed $CD8^+$ T cells activity through epigenetically inhibiting *CXCL16*

To elucidate the specific mechanism through which ZEB1 negatively regulates *CXCL16* expression to

decrease response to chemoimmunotherapy, we conducted a luciferase reporter assay to assess the role of ZEB1 on *CXCL16* transcriptional regulation. The results showed that *ZEB1* KD increased *CXCL16* mRNA level but did not affect *CXCL16* promoter activity (Figure 5I and Supplemental Figure 5, R and S), suggesting that ZEB1 may regulate CXCL16 in an epigenetically dependent manner. We further investigated the modification of the *CXCL16* promoter using CUT&Tag sequencing (CUT&Tag-seq). AsPC-1-R cells showed a clearly reduced level of H3K27ac in the *CXCL16* promoter region, while the H3K4me level only showed a slight reduction (Figure 5J). These findings imply that histone acetylation predominantly regulates CXCL16 expression in PC. CUT&Tag qPCR further confirmed a lower enrichment of H3K27ac signal in AsPC-1-R cells compared to the parental cells, while *ZEB1* KD partially restored the H3K27ac enrichment (Figure 5K). Next, we sought to elucidate the mechanism by which ZEB1 modulates H3K27 acetylation at the *CXCL16* promoter. Given that histone deacetylase 1 (HDAC1) is a well-characterized co-repressor of ZEB1 and facilitates ZEB1-mediated deacetylation of downstream targets, we performed HDAC1 CUT&Tag-qPCR in parental AsPC-1 cells and gemcitabine-resistant AsPC-1-R cells, with or without *ZEB1* knockdown. Strikingly, HDAC1 enrichment at the *CXCL16* promoter region was markedly elevated in gemcitabine-resistant cells, and this effect was almost completely abrogated upon *ZEB1* depletion (Figure 5L). Collectively, these findings revealed that the epigenetic modification of the *CXCL16* promoter by the HDAC1/ZEB1 complex contributes to *CXCL16* silencing in PC.

HDAC inhibitor synergizes with chemoimmunotherapy and CAR-T cell therapy in PC

To evaluate the translational potential of ZEB1 in PC chemoimmunotherapy, we selected Mocetinostat, an epigenetic inhibitor of ZEB1, to assess its synergistic effect with chemoimmunotherapy in PC. We established the orthotopic allograft mouse model and treated the mice with gemcitabine, gemcitabine+anti-PD1 (G+P), gemcitabine+Moce (G+M), and gemcitabine+anti-PD1+Moce (G+P+M), respectively. We found G+P plus 60mg/kg Moce treatment (G+P+M) significantly inhibited

the tumor growth; however, this regimen didn't significantly prolong the OS compared with G+M treatment (Supplemental Figure 6, A-C). Since previous clinical trials evaluating the efficacy of gemcitabine in combination with Moce in PC patients did not meet the primary endpoint due to severe side effects, we decided to explore whether a lower dosage of Moce (30mg/kg) might improve the efficacy. As expected, this treatment strategy significantly reduced tumor volume and improved OS (Figure 6, A and B, and Supplemental Figure 6D), while having markedly less severe side effects, as evidenced by tissue morphology and blood parameters associated with liver and kidney function (Supplemental Figure 6, E-F). To investigate the mechanism by which Moce enhances PC chemoimmunotherapy efficacy, we conducted flow cytometry and IHC to evaluate tumor-infiltrated immune cell profiling. The results showed that the triple-drug treatment led to a dramatic increase in the infiltration of $CD8^+$ T cells (Figure 6C and Supplemental Figure 6G). Meanwhile, neutrophils, often implicated in suppressing anticancer T cell activity across various cancer types, were significantly reduced following G+P+M treatment (Figure 6C and Supplemental Figure 6G). These results indicate that Moce increases chemoimmunotherapy response through remodeling the TIME. Chimeric antigen receptor (CAR)-engineered T cells (CAR-T cells) therapy has shown promising outcomes in hematological malignancies (48). However, the efficacy of CAR-T therapy in solid tumors remains limited, particularly in highly desmoplastic PC. To elucidate the impact of Moce on CAR-T cell therapy, we constructed patient-derived PC organoids (PDOs) and established CAR-T infiltrated and real-time killing models. High content confocal laser scanning microscope images and videos showed that Moce facilitated directional migration and augmented infiltration of CAR-T cells into the PDOs within the co-culture environment (Figure 6D). Notably, the synergistic effect of Moce and CAR-T cells induced dramatic PDO deformation, extensive cell lysis, and cell apoptosis, but the effect was not observed with CAR-T cells alone (Supplemental Figure 6, H-L). Given the substantial efficacy of Moce and G+P on TIME activation, a patient-derived organoid xenograft mouse model (PDOX) was established to investigate whether Moce enhances CAR-T cell therapy response in vivo. As shown

in Figure 6E-6I, treatment with Moce dramatically improved the anti-tumor efficacy of CAR-T therapy. Thus, Moce reinforces the anti-tumor immunity and enhances the efficacy of chemoimmunotherapy and CAR-T cell therapy in PC.

Moce enhances chemoimmunotherapy sensitivity by targeting HDAC1/2-ZEB1 complex

Next, we treated the resistant cells with Moce and found that Moce increased the sensitivity of AsPC-R cells to gemcitabine and activated $CD8^+$ T cells in vitro (Supplemental Figure 7, A-F). To determine whether the efficacy of Moce on PC response to chemoimmunotherapy depends on inhibiting the HDAC1/2-ZEB1 functional complex, we performed a co-immunoprecipitation (co-IP) assay. We found that ZEB1 can interact with HDAC1 and HDAC2 (Supplemental Figure 7G). Intriguingly, Moce reduced the stability of ZEB1 and HDAC1 but not HDAC2 (Supplemental Figure 7H). These results indicate that Moce promotes response to chemoimmunotherapy by disrupting the HDAC1-ZEB1 complex in PC.

ZEB1 and CXCL16 expression are positively correlated with gemcitabine resistance and associated with poor clinical outcomes

We explored the correlation between ZEB1 and CXCL16 expression, as well as $CD8^+$ T cell infiltration, and the sensitivity of gemcitabine in PC patients. In PC patients, ZEB1 expression was positively correlated with gemcitabine resistance, whereas CXCL16 and CD8 expression were negatively correlated (Figure 7A). We further validated these findings using scRNA-seq of tumor tissues from PC patients, demonstrating that those with higher CXCL16 expression were more sensitive to gemcitabine treatment (Figure 7, B-E, and Supplemental Figure 7, I-J). Collectively, our data highlight ZEB1 as a central regulator that modulates the efficacy of immunotherapy and gemcitabine in PC, through its epigenetic regulation of CXCL16 expression and the intratumoral balance of $CD8^+$ T cells and neutrophils (Figure 7F).

Discussion

Chemotherapy inadvertently promotes tumor immune escape, ultimately leading to treatment failure, recurrence, and metastasis. It's demonstrated that in gemcitabine-resistant PDAC cells, CMTM6 stabilizes PD-L1 expression and inhibits T-cell activity (49, 50); In addition, gemcitabine induces DNA damage response, activating APOBEC3C/3D enzymes which enhance DNA repair and upregulate immune checkpoint molecules PD-L1, consequently suppressing T-cell function and facilitating immune evasion (51); And, EVs secreted by chemotherapy-resistant cells transport miR-21-5p (known to target tumor suppressors like PDCD4) or PVT1, further inhibiting T-cell activity (52).

ZEB1 is one of the key transcription factors that promote cellular plasticity and tumor metastasis in PC (53, 54). Previous studies showed that ZEB1 induced gemcitabine resistance in PC by activating ITGA3-JNK signaling and downregulating *ENT1* (42). However, the role of ZEB1 in driving chemoimmunotherapy resistance remains elusive. We found that blocking ZEB1 enhanced the efficacy of chemotherapy and immunotherapy (anti-PD1 therapy and CAR-T therapy) by reprogramming the immune microenvironment of PC. Specifically, ZEB1 inhibition increased the infiltration of $CD8^+$ T cells while decreasing the infiltration of neutrophils in vivo. Mechanistically, ZEB1 binds with HDAC1 to regulate the chromatin accessibility of *CXCL16* through histone acetylation, which induces the imbalance of $CD8^+$ T cells and neutrophils. Furthermore, our study showed that $CD8^+$ T cells reversed chemoresistance by increasing ENT1 expression, echoing the feedforward loop between chemotherapy and immunotherapy. This work delineates the central role of ZEB1 in reprogramming the tumor immune microenvironment through epigenetic mechanisms, thereby identifying promising therapeutic targets for enhancing chemotherapy and immunotherapy in PC.

Epigenetic modification, such as acetylation, plays a critical role in driving treatment resistance (55, 56). HDAC1 is a co-transcriptional repressor of ZEB1. However, previous clinical trials evaluating HDAC inhibitors, including mocetinostat, either alone or in combination with chemotherapy or immune checkpoint inhibitors, have failed to demonstrate obvious efficacy in pancreatic cancer and

were frequently associated with dose-limiting toxicities, particularly at standard or high doses (57-59). In mouse models, we found that HDAC inhibitor showed better treatment response when combined with chemotherapy and immunotherapy. We proposed a potential treatment strategy by combining HDAC inhibitor with chemotherapy and immunotherapy, which achieved promising efficacy in PC. Chemokines are critical in regulating immune evasion by facilitating the communication between tumor cells and other cell types in microenvironment (60-64). We found that CXCL16 recruits and activates $CD8^+$ T cells, especially the $GZMA^+CD8^+$ T cells, a subpopulation of $CD8^+$ T cells that has potent cytotoxicity to tumor cells. $GZMA^+CD8^+$ T cells promote the pyroptosis of tumor cells via GSDMD. This is consistent with previous reports showing that cytotoxic lymphocytes can induce pyroptosis in target cells (17). Epigenetic modifications regulate the efficacy of immunotherapy by remodeling tumor immune microenvironment (65). We delved into the role of epigenetic modification in regulating CXCL16 expression and delineated that the HDAC1-ZEB1 complex promotes the deacetylation of *Cxcl16*, resulting in the decreased transcription and expression of CXCL16. This evidence supports the rationale of combining HDACi, chemotherapy, and immunotherapy for the treatment of PC.

Furthermore, we noticed the decreased infiltration of neutrophils in tumor microenvironment when blocking HDAC1 or ZEB1. Neutrophils induce cancer immune evasion by secreting immune-modulating cytokines, leading to the decreased treatment response of immunotherapy (66). Studies showed that suppressing the infiltration of neutrophils and MDSCs by inhibiting CXCR2 resulted in the synergistic anti-tumor immunity when combined with immunotherapy (61, 67). Intriguingly, senescence-like neutrophils are more potent in driving immunosuppression than their canonical counterparts (68). Moreover, HDAC inhibitor showed synergistic anti-tumor effect with CXCR2 inhibitor by eliminating the infiltration of senescence-like neutrophils in prostate cancer(68). Future studies may evaluate whether blocking HDAC and neutrophils would increase sensitivity to chemotherapy and immunotherapy in PC.

This study also has limitations. The mechanism by which ZEB1 mediates the upregulation of SPP1 remains unclear. Additionally, the potential of other HDAC inhibitors to enhance the efficacy of chemoimmunotherapy in PC warrants further investigation. Currently, no inhibitors are available that specifically target ZEB1. The development of a ZEB1-specific inhibitor would provide a valuable tool to further validate its role in mediating resistance to chemoimmunotherapy.

In conclusion, this study identifies a ZEB1-driven reprogramming of the tumor microenvironment that contributes to resistance to both immunotherapy and chemotherapy in pancreatic cancer (PC). While chemotherapy and immunotherapy primarily target tumor cells directly, HDAC inhibitors offer a promising synergistic strategy by modulating key components of the tumor immune microenvironment. These findings underscore the therapeutic potential of targeting epigenetic modifications, particularly histone acetylation, to overcome treatment resistance and improve outcomes in PC.

METHODS

Sex as a biological variable. Our study examined male and female animals, and similar findings are reported for both sexes.

PDOX mouse model establishment. PDOs were inoculated onto the back of NSG mice to establish the PDOX F1 generation, and subsequently, the F1 tumors were chopped into small pieces and inoculated onto the back of nude mice to generate the F2 generation. F3 generation was subsequently obtained with the same operation. The PDOX mouse model used in the experiments was the F3 generation.

Construction of Chimeric Antigen Receptor T-cell Therapy (CAR-T). The construction of EGFR-targeted chimeric antigen receptor T (CAR-T) cells was performed using a standardized protocol. Initial validation of EGFR surface expression was conducted via flow cytometric analysis using APC-conjugated anti-EGFR monoclonal antibody (ABclonal, AB_3662630), demonstrating >90%

positivity in both the AsPC-1 cell line and patient-derived organoid models. A second-generation CAR construct was engineered, comprising: an anti-EGFR single-chain variable fragment derived from cetuximab; CD8α extracellular hinge and transmembrane domains; 4-1BB (CD137) costimulatory domain; CD3ζ signaling domain; and T2A-linked GFP reporter. The construct was cloned into pLVX-EF1α lentiviral vector and sequence-verified. Lentiviral particles were produced by triple transfection of 293T cells with the CAR transfer vector, psPAX2 packaging plasmid, and pMD2.G envelope plasmid, followed by ultracentrifugation to achieve final titers of 1×10^8 transducing units/mL. For CAR-T cell generation, $CD8^+$ T lymphocytes were isolated from healthy donor PBMCs via negative selection (EasySep™ Human $CD8^+$ T Cell Isolation Kit, STEMCELL Technologies), activated with anti-CD3/CD28 Dynabeads at 1:1 bead-to-cell ratio in the presence of 100 IU/mL recombinant human IL-2, and lentivirus was added to infect the $CD8^+$ T cells. One week later, the infection efficiency was assessed by measuring the percentage of cells exhibiting green fluorescence (GFP) using flow cytometry. The positive rate of EGFR-CAR-T cells was 50%.

10x scRNA sequencing. According to the user manual (CG00315) for the 10x Genomics Chromium Next GEM Single Cell 3′ Kit v3.1 (1000268), the single cell suspension was immediately loaded onto a chip to generate GEMs (Gel Bead-in-Emulsion) droplets using the 10x Chromium Controller. Reverse transcription, cDNA amplification, and DNA library construction were performed sequentially according to the protocol. The concentration and fragment size of the libraries were measured using the Invitrogen Qubit 4.0 and Agilent 4150 TapeStation. High-throughput sequencing was conducted using high-throughput paired-end 150 bp (PE-150) mode. This work is assisted by OE Biotech Co., Ltd. (Shanghai, China).

Publicly available scRNA-seq data. FASTQ files of the scRNA-seq data from human PDAC were obtained from Peng et al.(69) (GSA: CRA001160). De-identified clinical information was kindly provided by the authors.

ATAC-seq, CUT&TAG-seq, RNA-seq and Joint analysis. ATAC-seq: Collected AsPC-1 and AsPC GEM cells to prepare cell suspensions and obtain cell nuclei. Then, added Tn5 transposase to cleave the DNA into fragments. PCR amplification of DNA fragments and sequencing on Illumina Novo sequencing platform. CUT&TAG-seq: CUT&TAG was performed in AsPC-1 and AsPC-GEM cells by using the anti-H3K27ac (CST, 8173), anti-H3K4me (CST, 9751) antibody. The experimental process is as described earlier, and finally, DNA libraries were sequenced on illumina Nova-seq platform. RNA-seq: Total RNA was extracted using the Trizol (Invitrogen) method and RNA purity was detected using NanoDrop One (Thermo Fisher Scientific). Next, mRNA was enriched (T oligo), purified, and a library was constructed. Subsequently, sequencing was performed on MGI-SEQ 2000 platform. Perform joint analysis of ATAC-seq, CUT&TAG-seq and RNA-seq data by Frasergen Bioinformatics Co., Ltd. (Wuhan, China).

***Statistics*.** Statistical analyses were performed using GraphPad Prism 9 and R 4.1.2. All animal experiments' data were presented as the mean ± SD and analyzed by one-way ANOVA with Tukey's multiple comparisons test or unpaired, 2-tailed Student's t test. *P* value less than 0.05 was considered statistically significant. Animal survival analysis was analyzed by log-rank test. More descriptions about statistical details are indicated in the methods and figure legends. Error bars in the experiments indicate standard error of the mean ± SEM or standard deviation ± SD.

Study approval. This study was approved by the Institutional Review Board (IRB) at PUMC hospital. Banked de-identified tissues were used. Written consent from all subjects was obtained. All animal experiments were approved by the Institutional Animal Care and Use Committee (IACUC) at PUMC hospital.

Data availability. Values for data points in the figures are available in the Supporting Data Values file. ScRNA-seq data generated in this study are available in Gene Expression Omnibus database with accession number GSE281084, and the spatial transcriptomics sequencing data are available with

accession number GSE281083. This study did not generate new unique codes. Any additional information required to reanalyze the data reported in this paper will be fulfilled by the corresponding authors upon reasonable request.

Author Contributions

M Liu and ML designed and supervised the study. SZ, YH, ZZ, GL, CZ, YG, FW, YY, HQ, H Zhang, H Zhao and WW performed the experiments, analyzed the data and contributed to the visualization of the data. M Liu and ML provided the resources. M Liu and YH acquired the funding. SZ, YH and ZZ wrote the original drafts. GL, CZ, YG, FW, YY, HQ, H Zhang, H Zhao, WW, ML and M Liu reviewed and edit the manuscript. Co-first authorship was determined by their equal contribution to this study, with SZ listed as the first author because he took the leading role in performing experiments, organizing the figures and writing the original draft.

Acknowledgements

The study was supported by the National Natural Science Foundation of China (nos. 82273452 and 92474301 to M.Liu), the National Key Research and Development Program of China (nos. 2023YFC2413200 and 2023YFC2413205 to M.Liu), the Chinese Academy of Medical Sciences Innovation Fund for Medical Sciences (nos. 2023-I2M-2-004 to M.Liu), the Non-profit Central Research Institute Fund of Chinese Academy of Medical Sciences (nos. 2022-RC310-01 to M.Liu), the Beijing Hope Run Special Fund of Cancer Foundation of China (nos. LC2022R05 to M.Liu), the National Natural Science Foundation of China (nos. 82403706 to Y.H.), the Fundamental Research Funds for the Central Universities (nos. 3332024047 to Y.H.), and the Postdoctoral Fellowship Program of CPSF under Grant Number GZC20240140.

References

1. Rahib L, Wehner MR, Matrisian LM, and Nead KT. Estimated Projection of US Cancer Incidence and Death to 2040. *JAMA Netw Open.* 2021;4(4):e214708.
2. Pishvaian MJ, Blais EM, Brody JR, Lyons E, DeArbeloa P, Hendifar A, et al. Overall survival in patients with pancreatic cancer receiving matched therapies following molecular profiling: a retrospective analysis of the Know Your Tumor registry trial. *Lancet Oncol.* 2020;21(4):508-18.
3. Hu ZI, and O'Reilly EM. Therapeutic developments in pancreatic cancer. *Nat Rev Gastroenterol Hepatol.* 2024;21(1):7-24.
4. Zhou Z, and Li M. Targeted therapies for cancer. *BMC Med.* 2022;20(1):90.
5. Iacobuzio-Donahue CA, Litchfield K, and Swanton C. Intratumor heterogeneity reflects clinical disease course. *Nat Cancer.* 2020;1(1):3-6.
6. Grunwald BT, Devisme A, Andrieux G, Vyas F, Aliar K, McCloskey CW, et al. Spatially confined sub-tumor microenvironments in pancreatic cancer. *Cell.* 2021;184(22):5577-92 e18.
7. Balachandran VP, Luksza M, Zhao JN, Makarov V, Moral JA, Remark R, et al. Identification of unique neoantigen qualities in long-term survivors of pancreatic cancer. *Nature.* 2017;551(7681):512-6.
8. Wang Z, Li B, Li S, Lin W, Wang Z, Wang S, et al. Metabolic control of CD47 expression through LAT2-mediated amino acid uptake promotes tumor immune evasion. *Nat Commun.* 2022;13(1):6308.
9. Yu L, Liebenberg K, Shen Y, Liu F, Xu Z, Hao X, et al. Tumor-derived arachidonic acid reprograms neutrophils to promote immune suppression and therapy resistance in triple-negative breast cancer. *Immunity.* 2025;58(4):909-25.e7.
10. Werba G, Weissinger D, Kawaler EA, Zhao E, Kalfakakou D, Dhara S, et al. Single-cell RNA sequencing reveals the effects of chemotherapy on human pancreatic adenocarcinoma and its

tumor microenvironment. *Nat Commun.* 2023;14(1):797.

11. Rohila D, Park IH, Pham TV, Weitz J, Hurtado de Mendoza T, Madheswaran S, et al. Syk Inhibition Reprograms Tumor-Associated Macrophages and Overcomes Gemcitabine-Induced Immunosuppression in Pancreatic Ductal Adenocarcinoma. *Cancer Res.* 2023;83(16):2675-89.
12. Ho WJ, Jaffee EM, and Zheng L. The tumour microenvironment in pancreatic cancer - clinical challenges and opportunities. *Nat Rev Clin Oncol.* 2020;17(9):527-40.
13. El-Tanani M, Rabbani SA, Babiker R, Rangraze I, Kapre S, Palakurthi SS, et al. Unraveling the tumor microenvironment: Insights into cancer metastasis and therapeutic strategies. *Cancer Lett.* 2024;591:216894.
14. Liu Y, Zhao Y, Song H, Li Y, Liu Z, Ye Z, et al. Metabolic reprogramming in tumor immune microenvironment: Impact on immune cell function and therapeutic implications. *Cancer Lett.* 2024;597:217076.
15. Zhou Z, Ren Y, Yang J, Liu M, Shi X, Luo W, et al. Acetyl-Coenzyme A Synthetase 2 Potentiates Macropinocytosis and Muscle Wasting Through Metabolic Reprogramming in Pancreatic Cancer. *Gastroenterology.* 2022;163(5):1281-93.e1.
16. Zhang R, Peng J, Zhang Y, Zheng K, Chen Y, Liu L, et al. Pancreatic cancer cell-derived migrasomes promote cancer progression by fostering an immunosuppressive tumor microenvironment. *Cancer Lett.* 2024;605:217289.
17. Zhou Z, He H, Wang K, Shi X, Wang Y, Su Y, et al. Granzyme A from cytotoxic lymphocytes cleaves GSDMB to trigger pyroptosis in target cells. *Science.* 2020;368(6494).
18. Liu Y, Fang Y, Chen X, Wang Z, Liang X, Zhang T, et al. Gasdermin E-mediated target cell pyroptosis by CAR T cells triggers cytokine release syndrome. *Sci Immunol.* 2020;5(43).
19. Zhang Z, Zhang Y, Xia S, Kong Q, Li S, Liu X, et al. Gasdermin E suppresses tumour growth by activating anti-tumour immunity. *Nature.* 2020;579(7799):415-20.
20. Wang Y, Gao W, Shi X, Ding J, Liu W, He H, et al. Chemotherapy drugs induce pyroptosis

through caspase-3 cleavage of a gasdermin. *Nature.* 2017;547(7661):99-103.

21. Zhang Y, Naderi Yeganeh P, Zhang H, Wang SY, Li Z, Gu B, et al. Tumor editing suppresses innate and adaptive antitumor immunity and is reversed by inhibiting DNA methylation. *Nat Immunol.* 2024;25(10):1858-70.

22. Griffin GK, Wu J, Iracheta-Vellve A, Patti JC, Hsu J, Davis T, et al. Epigenetic silencing by SETDB1 suppresses tumour intrinsic immunogenicity. *Nature.* 2021;595(7866):309-14.

23. Chen YX, Wang ZX, Jin Y, Zhao Q, Liu ZX, Zuo ZX, et al. An immunogenic and oncogenic feature-based classification for chemotherapy plus PD-1 blockade in advanced esophageal squamous cell carcinoma. *Cancer Cell.* 2023;41(5):919-32 e5.

24. Jones PA, Ohtani H, Chakravarthy A, and De Carvalho DD. Epigenetic therapy in immune-oncology. *Nat Rev Cancer.* 2019;19(3):151-61.

25. Topper MJ, Vaz M, Marrone KA, Brahmer JR, and Baylin SB. The emerging role of epigenetic therapeutics in immuno-oncology. *Nat Rev Clin Oncol.* 2020;17(2):75-90.

26. Ren J, Ren B, Liu X, Cui M, Fang Y, Wang X, et al. Crosstalk between metabolic remodeling and epigenetic reprogramming: A new perspective on pancreatic cancer. *Cancer Lett.* 2024;587:216649.

27. Wang X, Liu X, Xiao R, Fang Y, Zhou F, Gu M, et al. Histone lactylation dynamics: Unlocking the triad of metabolism, epigenetics, and immune regulation in metastatic cascade of pancreatic cancer. *Cancer Lett.* 2024;598:217117.

28. Chen Q, Yuan H, Bronze MS, and Li M. Targeting lactylation and the STAT3/CCL2 axis to overcome immunotherapy resistance in pancreatic ductal adenocarcinoma. *J Clin Invest.* 2025;135(7).

29. Sun K, Zhang X, Shi J, Huang J, Wang S, Li X, et al. Elevated protein lactylation promotes immunosuppressive microenvironment and therapeutic resistance in pancreatic ductal adenocarcinoma. *J Clin Invest.* 2025;135(7).

30. Liang G, Oh TG, Hah N, Tiriac H, Shi Y, Truitt ML, et al. Inhibiting stromal Class I HDACs curbs pancreatic cancer progression. *Nat Commun.* 2023;14(1):7791.
31. Roca MS, Moccia T, Iannelli F, Testa C, Vitagliano C, Minopoli M, et al. HDAC class I inhibitor domatinostat sensitizes pancreatic cancer to chemotherapy by targeting cancer stem cell compartment via FOXM1 modulation. *J Exp Clin Cancer Res.* 2022;41(1):83.
32. Tu Y, Wu H, Zhong C, Liu Y, Xiong Z, Chen S, et al. Pharmacological activation of STAT1-GSDME pyroptotic circuitry reinforces epigenetic immunotherapy for hepatocellular carcinoma. *Gut.* 2025;74(4):613-27.
33. Xu T, Fang Y, Gu Y, Xu D, Hu T, Yu T, et al. HDAC inhibitor SAHA enhances antitumor immunity via the HDAC1/JAK1/FGL1 axis in lung adenocarcinoma. *J Immunother Cancer.* 2024;12(10).
34. Wang F, Jin Y, Wang M, Luo HY, Fang WJ, Wang YN, et al. Combined anti-PD-1, HDAC inhibitor and anti-VEGF for MSS/pMMR colorectal cancer: a randomized phase 2 trial. *Nat Med.* 2024;30(4):1035-43.
35. Wu M, Hanly A, Gibson F, Fisher R, Rogers S, Park K, et al. The CoREST repressor complex mediates phenotype switching and therapy resistance in melanoma. *J Clin Invest.* 2024;134(6).
36. Winkler J, Tan W, Diadhiou CM, McGinnis CS, Abbasi A, Hasnain S, et al. Single-cell analysis of breast cancer metastasis reveals epithelial-mesenchymal plasticity signatures associated with poor outcomes. *J Clin Invest.* 2024;134(17).
37. Susanto O, Stewart SE, Voskoboinik I, Brasacchio D, Hagn M, Ellis S, et al. Mouse granzyme A induces a novel death with writhing morphology that is mechanistically distinct from granzyme B-induced apoptosis. *Cell Death Differ.* 2013;20(9):1183-93.
38. Lieberman J. Granzyme A activates another way to die. *Immunol Rev.* 2010;235(1):93-104.
39. Laklai H, Miroshnikova YA, Pickup MW, Collisson EA, Kim GE, Barrett AS, et al. Author Correction: Genotype tunes pancreatic ductal adenocarcinoma tissue tension to induce

564 matricellular fibrosis and tumor progression. *Nat Med.* 2024;30(3):908.
565 40. Balachandran VP, Beatty GL, and Dougan SK. Broadening the Impact of Immunotherapy to
566 Pancreatic Cancer: Challenges and Opportunities. *Gastroenterology.* 2019;156(7):2056-72.
567 41. Koikawa K, Kibe S, Suizu F, Sekino N, Kim N, Manz TD, et al. Targeting Pin1 renders
568 pancreatic cancer eradicable by synergizing with immunochemotherapy. *Cell.*
569 2021;184(18):4753-71 e27.
570 42. Liu M, Zhang Y, Yang J, Cui X, Zhou Z, Zhan H, et al. ZIP4 Increases Expression of
571 Transcription Factor ZEB1 to Promote Integrin alpha3beta1 Signaling and Inhibit Expression
572 of the Gemcitabine Transporter ENT1 in Pancreatic Cancer Cells. *Gastroenterology.*
573 2020;158(3):679-92 e1.
574 43. Wang X, Chen Z, Nie D, Zeng X, Zhong M, Liu X, et al. CASP1 is a target for combination
575 therapy in pancreatic cancer. *Eur J Pharmacol.* 2023;961:176175.
576 44. Quail DF, Amulic B, Aziz M, Barnes BJ, Eruslanov E, Fridlender ZG, et al. Neutrophil
577 phenotypes and functions in cancer: A consensus statement. *J Exp Med.* 2022;219(6).
578 45. Wang B, Wang Y, Sun X, Deng G, Huang W, Wu X, et al. CXCR6 is required for antitumor
579 efficacy of intratumoral CD8(+) T cell. *J Immunother Cancer.* 2021;9(8).
580 46. Lesch S, Blumenberg V, Stoiber S, Gottschlich A, Ogonek J, Cadilha BL, et al. T cells armed
581 with C-X-C chemokine receptor type 6 enhance adoptive cell therapy for pancreatic tumours.
582 *Nat Biomed Eng.* 2021;5(11):1246-60.
583 47. Di Pilato M, Kfuri-Rubens R, Pruessmann JN, Ozga AJ, Messemaker M, Cadilha BL, et al.
584 CXCR6 positions cytotoxic T cells to receive critical survival signals in the tumor
585 microenvironment. *Cell.* 2021;184(17):4512-30 e22.
586 48. Sheridan C. First approval in sight for Novartis' CAR-T therapy after panel vote. *Nat*
587 *Biotechnol.* 2017;35(8):691-3.
588 49. Miao B, Hu Z, Mezzadra R, Hoeijmakers L, Fauster A, Du S, et al. CMTM6 shapes antitumor

T cell response through modulating protein expression of CD58 and PD-L1. *Cancer Cell.* 2023;41(10):1817-28.e9.

50. Zhu YQ, Huang Y, Shi YH, Huang CS, Zhao GY, Liu ZD, et al. Epigenetic Activation of the CMTM6-IGF2BP1-EP300 Positive Feedback Loop Drives Gemcitabine Resistance in Pancreatic Ductal Adenocarcinoma. *Adv Sci (Weinh).* 2024;11(47):e2406714.

51. Ubhi T, Zaslaver O, Quaile AT, Plenker D, Cao P, Pham NA, et al. Cytidine deaminases APOBEC3C and APOBEC3D promote DNA replication stress resistance in pancreatic cancer cells. *Nat Cancer.* 2024;5(6):895-915.

52. Zhou C, Yi C, Yi Y, Qin W, Yan Y, Dong X, et al. LncRNA PVT1 promotes gemcitabine resistance of pancreatic cancer via activating Wnt/β-catenin and autophagy pathway through modulating the miR-619-5p/Pygo2 and miR-619-5p/ATG14 axes. *Mol Cancer.* 2020;19(1):118.

53. Liu M, Yang J, Zhang Y, Zhou Z, Cui X, Zhang L, et al. ZIP4 Promotes Pancreatic Cancer Progression by Repressing ZO-1 and Claudin-1 through a ZEB1-Dependent Transcriptional Mechanism. *Clin Cancer Res.* 2018;24(13):3186-96.

54. Liu M, Zhang Y, Yang J, Zhan H, Zhou Z, Jiang Y, et al. Zinc-Dependent Regulation of ZEB1 and YAP1 Coactivation Promotes Epithelial-Mesenchymal Transition Plasticity and Metastasis in Pancreatic Cancer. *Gastroenterology.* 2021;160(5):1771-83 e1.

55. Morel KL, Germán B, Hamid AA, Nanda JS, Linder S, Bergman AM, et al. Low tristetraprolin expression activates phenotypic plasticity and primes transition to lethal prostate cancer in mice. *J Clin Invest.* 2024;135(2).

56. Bergamasco MI, Vanyai HK, Garnham AL, Geoghegan ND, Vogel AP, Eccles S, et al. Increasing histone acetylation improves sociability and restores learning and memory in KAT6B-haploinsufficient mice. *J Clin Invest.* 2024;134(7).

57. Chan E, Chiorean EG, O'Dwyer PJ, Gabrail NY, Alcindor T, Potvin D, et al. Phase I/II study of mocetinostat in combination with gemcitabine for patients with advanced pancreatic cancer

and other advanced solid tumors. *Cancer Chemother Pharmacol.* 2018;81(2):355-64.

58. Weber JS, Levinson BA, Laino AS, Pavlick AC, and Woods DM. Clinical and immune correlate results from a phase 1b study of the histone deacetylase inhibitor mocetinostat with ipilimumab and nivolumab in unresectable stage III/IV melanoma. *Melanoma Res.* 2022;32(5):324-33.

59. Younes A, Oki Y, Bociek RG, Kuruvilla J, Fanale M, Neelapu S, et al. Mocetinostat for relapsed classical Hodgkin's lymphoma: an open-label, single-arm, phase 2 trial. *Lancet Oncol.* 2011;12(13):1222-8.

60. Liu M, Ren Y, Zhou Z, Yang J, Shi X, Cai Y, et al. The crosstalk between macrophages and cancer cells potentiates pancreatic cancer cachexia. *Cancer Cell.* 2024.

61. Steele CW, Karim SA, Leach JDG, Bailey P, Upstill-Goddard R, Rishi L, et al. CXCR2 Inhibition Profoundly Suppresses Metastases and Augments Immunotherapy in Pancreatic Ductal Adenocarcinoma. *Cancer Cell.* 2016;29(6):832-45.

62. Schalper KA, Carleton M, Zhou M, Chen T, Feng Y, Huang SP, et al. Elevated serum interleukin-8 is associated with enhanced intratumor neutrophils and reduced clinical benefit of immune-checkpoint inhibitors. *Nat Med.* 2020;26(5):688-92.

63. Yuen KC, Liu LF, Gupta V, Madireddi S, Keerthivasan S, Li C, et al. High systemic and tumor-associated IL-8 correlates with reduced clinical benefit of PD-L1 blockade. *Nat Med.* 2020;26(5):693-8.

64. Zhou Z, Xia G, Xiang Z, Liu M, Wei Z, Yan J, et al. A C-X-C Chemokine Receptor Type 2-Dominated Cross-talk between Tumor Cells and Macrophages Drives Gastric Cancer Metastasis. *Clin Cancer Res.* 2019;25(11):3317-28.

65. Peng D, Kryczek I, Nagarsheth N, Zhao L, Wei S, Wang W, et al. Epigenetic silencing of TH1-type chemokines shapes tumour immunity and immunotherapy. *Nature.* 2015;527(7577):249-53.

66. Kargl J, Zhu X, Zhang H, Yang GHY, Friesen TJ, Shipley M, et al. Neutrophil content predicts lymphocyte depletion and anti-PD1 treatment failure in NSCLC. *JCI Insight.* 2019;4(24).

67. Xie Y, Zhou T, Li X, Zhao K, Bai W, Hou X, et al. Targeting ESE3/EHF With Nifurtimox Inhibits CXCR2(+) Neutrophil Infiltration and Overcomes Pancreatic Cancer Resistance to Chemotherapy and Immunotherapy. *Gastroenterology.* 2024;167(2):281-97.

68. Bancaro N, Cali B, Troiani M, Elia AR, Arzola RA, Attanasio G, et al. Apolipoprotein E induces pathogenic senescent-like myeloid cells in prostate cancer. *Cancer Cell.* 2023;41(3):602-19 e11.

69. Peng J, Sun BF, Chen CY, Zhou JY, Chen YS, Chen H, et al. Single-cell RNA-seq highlights intra-tumoral heterogeneity and malignant progression in pancreatic ductal adenocarcinoma. *Cell Res.* 2019;29(9):725-38.

Figure Legends

Figure 1. Blocking of Zeb1 enhances gemcitabine efficacy through activation of immune microenvironment of pancreatic cancer. (**A** and **B**) Tumor images and weight of orthotopic allograft mouse model (immune competent and immune deficient) established from KPC-shV and KPC-sh*Zeb1* cells and treated with gemcitabine (50 mg/kg) three times a week (n=3). (**C** and **D**) Tumor images and weight of orthotopic allograft mouse model established from KPC-shV and KPC-sh*Zeb1* cells in each treatment condition (n=5). (**E**) Survival of orthotopic allograft mouse model established from KPC-shV and KPC-sh*Zeb1* cells in each treatment condition (n=6-10). (**F-G**) Tumor images and weight of orthotopic allograft mouse model established from KPC-shV and KPC-sh*Zeb1* cells and treated with gemcitabine (50 mg/kg) and anti-Pd1 (10 mg/kg) three times a week (n=6). (**H**) The uniform manifold approximation and projection (UMAP) plot of scRNA-seq data derived from orthotopic allograft mouse model reveals the presence of 10 distinct cell types. Cells are colored by cell types. (**I**) UMAP plot displays the distribution and subclustering of T and NK cell subsets. (**J**) Stacked histogram shows the proportion of each T/NK cluster between KPC-shV and KPC-sh*Zeb1* mice tumor tissues. (**K**) Circle plots depict the strength of cell-cell interactions between subclusters of T/NK cells and tumor cells, as identified through CellChat analysis. The edge weights and numerical values indicate the strength score of these interactions, while the direction of the arrows denotes the cell clusters responsible for signaling release and reception. *$P < 0.05$, **$P < 0.01$, and ***$P < 0.001$, by unpaired, 2-tailed Student's *t* test (**B**), one-way ANOVA with Tukey's multiple comparisons test (**D** and **G**) and log-rank test (**E**). Data represent the mean ± SD in **B**, **D** and **G**.

Figure 2. Increased infiltration of *Gzma*$^+$ CD8$^+$ T cells in tumor tissue with *Zeb1* knockdown.

(**A**) UMAP reveals that CD8$^+$ T cells can be classified into four distinct major subtypes. (**B**) Density plot shows the expression of the *Gzma* gene, with brighter colors indicating higher expression. *Gzma* mainly expressed in the *Gzma*$^+$ effector CD8$^+$ T cell subset. (**C**) The bar plot compares the percentage

of *Gzma*$^+$ effector CD8$^+$ T cells within the total Cd45$^+$ population between the KPC-shV and KPC-sh*Zeb1* groups. (**D**) The number of inferred significant ligand-receptor (LR) pairs between any two cell types based on single-cell analysis data. (**E**) MIF of mouse tumor tissues is shown in the top left (scale bar 2mm) and top right panels (scale bar 200 μm). The bottom left and bottom right panels display the marker gene set scores for CD8$^+$ T cells based on spatial transcriptomics data. Brighter colors indicate higher scores, suggesting a greater abundance of CD8$^+$ T cells in those regions. (**F**) Spatial transcriptome sequencing displays the distribution of four major annotated cell types between the control and experiment groups. (**G** and **H**) Circle plots show the number and the strength score of LR among four cell types across two groups, based on spatial transcriptome data. (**I**) Specifically, the interaction strength of GZMA-related LR pairs is dramatically increased in the KPC-sh*Zeb1* group.

Figure 3. Blocking of ZEB1 enhances the anti-tumor activity of CD8$^+$ T cells. (**A**) The CD8$^+$ T cells migration assay. (**B**) Detection of the level of activation markers of mouse CD8$^+$ T cells by qPCR after co-culturing with KPC-shV, sh*Zeb1* cells for 48h. (**C**) Flow cytometry analysis of the apoptotic rate of human CD8$^+$ T cells after co-culturing with AsPC-R-shV, sh*ZEB1* cells. (**D**) Western blot detection of apoptotic markers in human CD8$^+$ T cells after co-culturing with AsPC-R-shV, sh*ZEB1* cells. (**E**) Specific lysis of AsPC-R-shV-luciferase and AsPC-R-sh*ZEB1*-luciferase cells after co-culturing with CAR-T for 48h. (**F**) Detection of specific lysis of KPC-shV-*Ova*-luciferase and KPC-sh*Zeb1*-*Ova*-luciferase after co-cultured with mouse *Ot1*-CD8$^+$ T cells for 24h. (**G** and **H**) Tumor images and weight of orthotopic allograft mouse model established from KPC-shV-*Ova* and KPC-sh*Zeb1*-*Ova* cells and treated with mouse *Ot1*-CD8$^+$ T cells (n=3-5). (**I**) Detection of the expression of ENT1 in AsPC-R-shV, sh*ZEB1* cells after treated with CD8$^+$ T conditioned medium for 48h. (**J**) Representative cells images of AsPC-R-shV, sh*ZEB1* after treated with gemcitabine (1000 nM) and conditioned medium of CD8$^+$ T for 48h (n=3). Cells were labeled using the calcium ion probe Calbryte 590 and the red fluorescence signal represents pyroptosis cells. Scale bar=50 μm. (**K**) Detection of pyroptosis proteins in AsPC-R-shV, sh*ZEB1* cells after treated with gemcitabine (1000nM) and co-

cultured with $CD8^+$ T cells. Data are representative of at least 3 (**A**, **B**, **C**, **D**, **E**, **F**, **I** and **K**) independent experiments. *$P < 0.05$, **$P < 0.01$, and ***$P < 0.001$, by unpaired, 2-tailed Student's *t* test (**A**, **B** and **C**), 2-way ANOVA (**E** and **F**) and one-way ANOVA with Tukey's multiple comparisons test (**H**). Data represent the mean ± SD in **A**, **B**, **C** and **H**, the mean ± SEM in **E** and **F**.

Figure 4. Zeb1 promotes neutrophil recruitment and drives their polarization toward an immunosuppressive phenotype. (**A**) Circle plots compare the strengths of cell-cell interactions between granulocytes and other cell types. (**B**) Neutrophil migration assay. Relative migration of mouse neutrophils after co-culture with KPC-shV, sh*Zeb1* cells for 12h. (**C**) The violin plot shows the AUCell scores of the N1 and N2 gene sets in neutrophils derived from shV and sh*Zeb1* models. (**D**) Neutrophil activation. Detection of N1 polarization markers (*Icam, Cxcl10, Tnfa*) and N2 polarization marker *Cxcr2* in neutrophils by qPCR after co-culturing with KPC-shV or sh*Zeb1* cells for 12h. (**E**) Relative migration of mouse $CD8^+$ T cells after co-culturing with neutrophils. (**F**) Schematic of a three-cell co-cultured system. (**G**) $CD8^+$ T cells were isolated from the three cell co-cultured systems, and the levels of activation markers were detected by qPCR. (**H**) Neutrophils were isolated from the three cell co-cultured systems, and the level of N1 and N2 polarization markers were detected by qPCR. (**I** and **J**) Tumor images and weight of orthotopic allograft mouse model established from KPC-shV and KPC-sh*Zeb1* cells and treated with gemcitabine (50 mg/kg) and anti-Ly6g (25 μg) three times a week (n=5). Data are representative of at least 3 (**B**, **D**, **E**, **G** and **H**) independent experiments. *$P < 0.05$, **$P < 0.01$, and ***$P < 0.001$, by unpaired, 2-tailed Student's *t* test (**B**, **D**, **E**, **G** and **H**), Wilcoxon rank-sum test (**C**) and one-way ANOVA with Tukey's multiple comparisons test (**J**). Data represent the mean ± SD in **B**, **D**, **E**, **G**, **H** and **J**.

Figure 5. ZEB1/HDAC1 inhibits the recruitment and function of $CD8^+$ T cells by epigenetically regulating CXCL16. (**A**) The circle plot shows the inferred *Cxcl16-Cxcr6* signaling network between each $CD8^+$ T cell subcluster and tumor cells. Edge weights represent the strength of the interactions. (**B**) Relative migration of mouse $CD8^+$ T cells, which were co-cultured with KPC-shV-shV, sh*Zeb1*-

shV, KPC-sh*Zeb1*-sh*Cxcl16* cells for 48h. (**C**) Detection of activation markers in mouse $CD8^+$ T cells, which were co-cultured with tumor cells for 48h. (**D**) Detection of specific lysis of tumor cells after co-culturing with mouse *Ot1*-$CD8^+$ T cells for 24h. (**E** and **F**) Tumor images and weight of orthotopic allograft mouse model established from indicated cell lines and treated with gemcitabine (50 mg/kg) three times a week (n=5). (**G** and **H**) Tumor images and weight of orthotopic allograft mouse model established from indicated cell lines and treated with mouse *Ot1*-$CD8^+$ T cells (n=3). (**I**) Relative mRNA level of *ZEB1* and *CXCL16* in AsPC-R-shV and sh*ZEB1* cells. (**J**) ATAC-seq, Cut&tag-seq of H3K27ac, Cut&tag-seq of H3K4me, and RNA-seq showed changes in chromatin openness, transcriptional activity, and apparent modification levels in the *CXCL16* promoter region and gene body region. (**K** and **L**) Cut&tag-qPCR assay of the *CXCL16* promoter region in AsPC-WT-siNC, AsPC-R-siNC, and AsPC-R-si*ZEB1* cells with antibodies against H3K27ac and HDAC1 (n=3). Data are representative of at least 3 (**B**, **C**, **D**, **I**, **K** and **L**) independent experiments. *$P < 0.05$, **$P < 0.01$, and ***$P < 0.001$, by one-way ANOVA with Tukey's multiple comparisons test (**B**, **C**, **F**, **H**, **I**, **K** and **L**) and 2-way ANOVA (**D**). Data represent the mean ± SD in **B**, **C**, **F**, **H**, **I**, **K** and **L**, the mean ± SEM in **D**.

Figure 6. Mocetinostat enhances the chemoimmunotherapy and CAR-T efficacy in PC. (**A**) Tumor images of orthotopic allograft mouse model established from KPC cells in each treatment condition: gemcitabine (50 mg/kg), gemcitabine+Moce (30 mg/kg), gemcitabine+Moce (30 mg/kg) + anti-PD1(10mg/kg), three times a week (n=6). (**B**) Survival of orthotopic allograft mouse model established from KPC cells in each treatment condition (n=10). (**C**) Flow cytometry analysis of the proportion of all T cells ($Cd45^+$, $Cd3^+$), $CD8^+$ T cells ($Cd3^+$, $Cd8^+$), and neutrophils ($Cd11b^+$, $Ly6g^+$) to total $Cd45^+$ cells in tumor tissue (n=3). (**D**) CAR-T infiltrated PDOs model: CAR-T was used to infect PDOs for 24h after the 24h of Moce (500 nM) treatment of PDOs (n=3). On the left is the 3D model synthesized by the algorithm. Green represents the PDOs, and red represents CAR-T. On the right is the 2D image of CAR-T infiltrating PDOs, CAR-T is shown in red with living cell dye. Scale

bar=20 μm. (**E**) Tumor images of the PDOX mouse model treated with CAR-T and Moce. (**F-G**) Tumor weight and volume of PDOX mouse model (n=3-5). (**H**) Representative H&E and Ki67 IHC staining in tumor tissues of the PDOX mouse model established from PC patients' organoids and treated with CAR-T and Moce (n=3). Scale bar=50 μm. (**I**) Flow cytometry analysis of the proportion of CAR-T cells (Human $CD3^+$ $CD8^+$) divided into total cells in mouse tumor tissues of PDOX mice after the treatment of CAR-T and Moce (n=3-5). *$P < 0.05$, **$P < 0.01$, and ***$P < 0.001$, by log-rank test (**B**), one-way ANOVA with Tukey's multiple comparisons test (**C**, **F** and **I**) and 2-way ANOVA (**G**). Data represent the mean ± SD in **C**, **F**, and **I**, the mean ± SEM in **G**.

Figure 7. ZEB1 and CXCL16 are associated with chemotherapy resistance, immunosuppression, and prognosis in PC patients. (**A**) Multiple Immunofluorescence of ZEB1, CXCL16, and CD8 in tumor tissues of chemo-sensitive and chemo-insensitive PC patients. Scale bar=50 μm. (**B**) Based on *CXCL16* expression, tumor cells were categorized into *CXCL16*-high and *CXCL16*-low groups. (**C**) Compared to the chemoresistant group, tumor cells with high *CXCL16* expression were predominantly found in the chemosensitive group. (**D**) The stacked histogram indicates a dramatic increase in the proportion of $CD8^+$ T cells in the chemosensitive group. (**E**) In the TCGA dataset, patients receiving adjuvant gemcitabine chemotherapy were stratified into high *CXCL16* expression (n=21) and low expression groups (n=44) based on the optimal cutoff value for *CXCL16* gene expression. Kaplan-Meier survival curves indicate that patients with high *CXCL16* expression exhibited a significantly better prognosis. (**F**) Schematic diagram. Crosstalk between PC cells, $CD8^+$ T cells, and neutrophils contributes to tumor immune invasion and gemcitabine resistance through ZEB1/HDAC1-CXCL16 signaling axis.

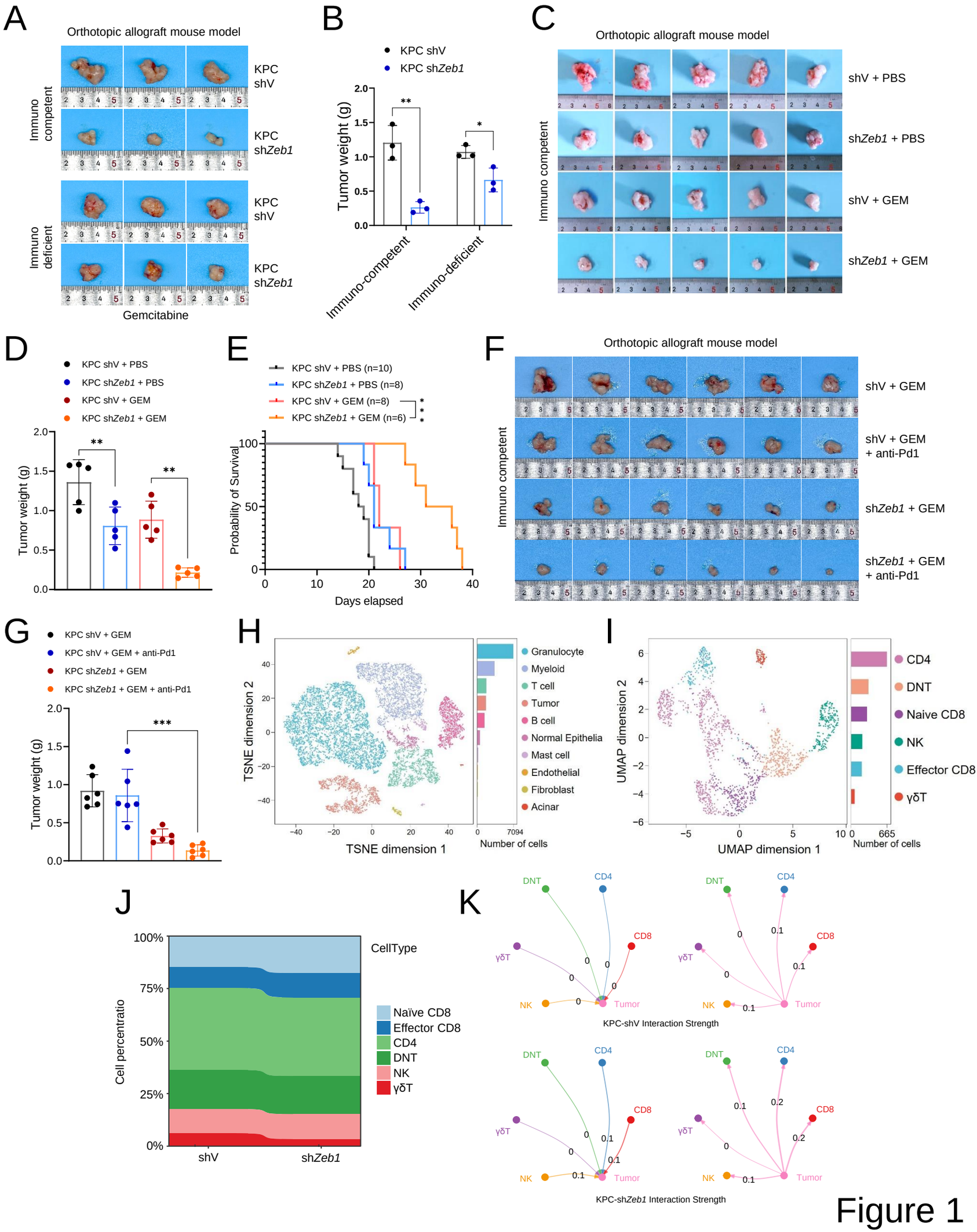
A
Orthotopic allograft mouse model
Immuno competent
Immuno deficient
KPC shV
KPC shZeb1
Gemcitabine
B
KPC shV
KPC shZeb1
Tumor weight (g)
Immuno-competent
Immuno-deficient
C
Orthotopic allograft mouse model
Immuno competent
shV + PBS
shZeb1 + PBS
shV + GEM
shZeb1 + GEM
D
KPC shV + PBS
KPC shZeb1 + PBS
KPC shV + GEM
KPC shZeb1 + GEM
Tumor weight (g)
E
KPC shV + PBS (n=10)
KPC shZeb1 + PBS (n=8)
KPC shV + GEM (n=8)
KPC shZeb1 + GEM (n=6)
Probability of Survival
Days elapsed
F
Orthotopic allograft mouse model
Immuno competent
shV + GEM
shV + GEM + anti-Pd1
shZeb1 + GEM
shZeb1 + GEM + anti-Pd1
G
KPC shV + GEM
KPC shV + GEM + anti-Pd1
KPC shZeb1 + GEM
KPC shZeb1 + GEM + anti-Pd1
Tumor weight (g)
H
TSNE dimension 1
TSNE dimension 2
Granulocyte
Myeloid
T cell
Tumor
B cell
Normal Epithelia
Mast cell
Endothelial
Fibroblast
Acinar
Number of cells
I
UMAP dimension 1
UMAP dimension 2
CD4
DNT
Naive CD8
NK
Effector CD8
γδT
Number of cells
J
Cell percentratio
CellType
Naïve CD8
Effector CD8
CD4
DNT
NK
γδT
shV
shZeb1
K
DNT
CD4
CD8
γδT
NK
Tumor
KPC-shV Interaction Strength
KPC-shZeb1 Interaction Strength

Figure 1

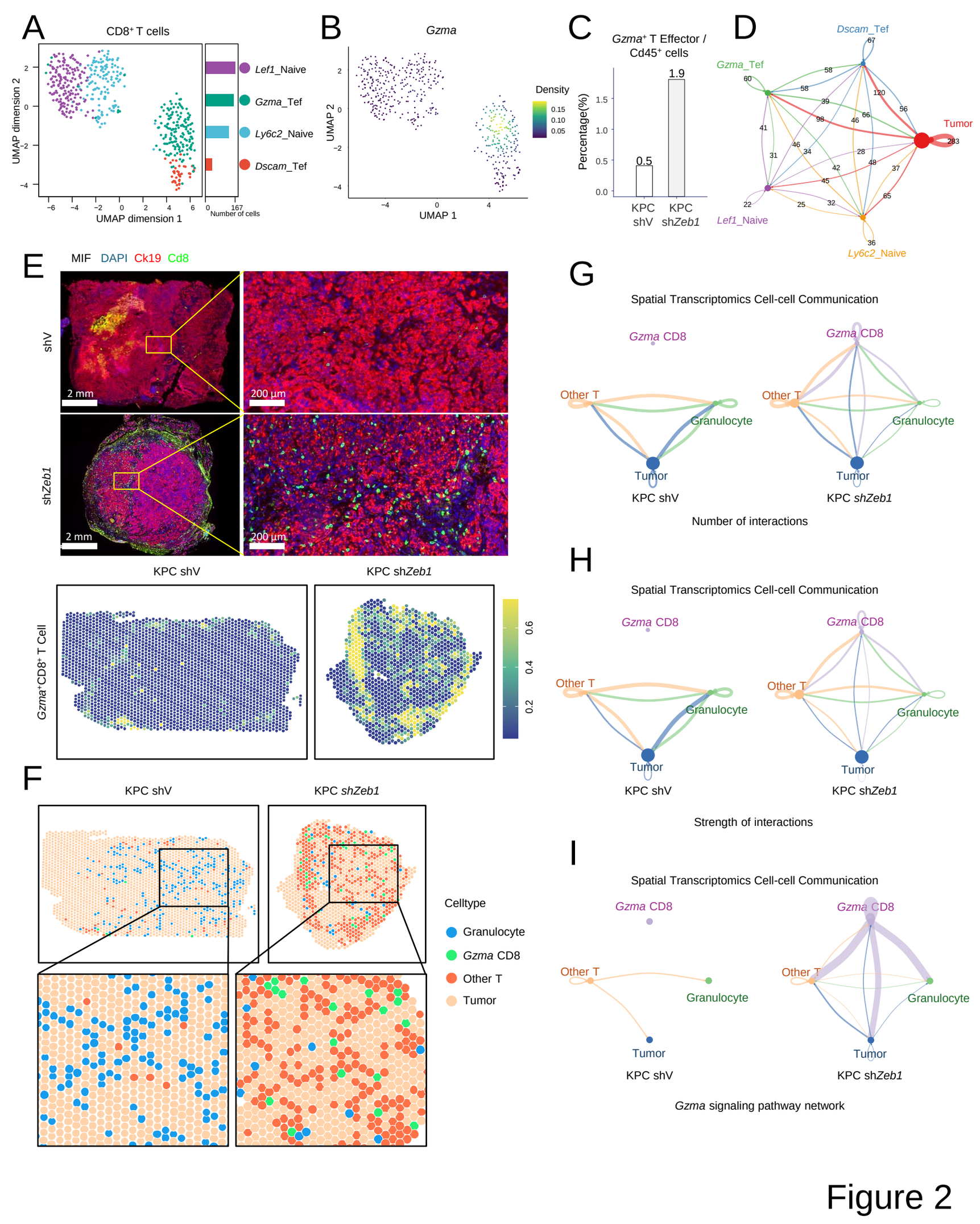
A
CD8⁺ T cells
UMAP dimension 2
UMAP dimension 1
Number of cells
Lef1_Naive
Gzma_Tef
Ly6c2_Naive
Dscam_Tef
B
Gzma
UMAP 2
UMAP 1
Density
C
Gzma⁺ T Effector / Cd45⁺ cells
Percentage(%)
1.9
0.5
KPC shV
KPC shZeb1
D
Dscam_Tef
Gzma_Tef
Tumor
Lef1_Naive
Ly6c2_Naive
E
MIF DAPI Ck19 Cd8
shV
shZeb1
2 mm
200 μm
KPC shV
KPC shZeb1
Gzma⁺CD8⁺ T Cell
F
KPC shV
KPC shZeb1
Celltype
Granulocyte
Gzma CD8
Other T
Tumor
G
Spatial Transcriptomics Cell-cell Communication
Gzma CD8
Other T
Granulocyte
Tumor
KPC shV
KPC shZeb1
Number of interactions
H
Spatial Transcriptomics Cell-cell Communication
Strength of interactions
I
Spatial Transcriptomics Cell-cell Communication
Gzma signaling pathway network

Figure 2

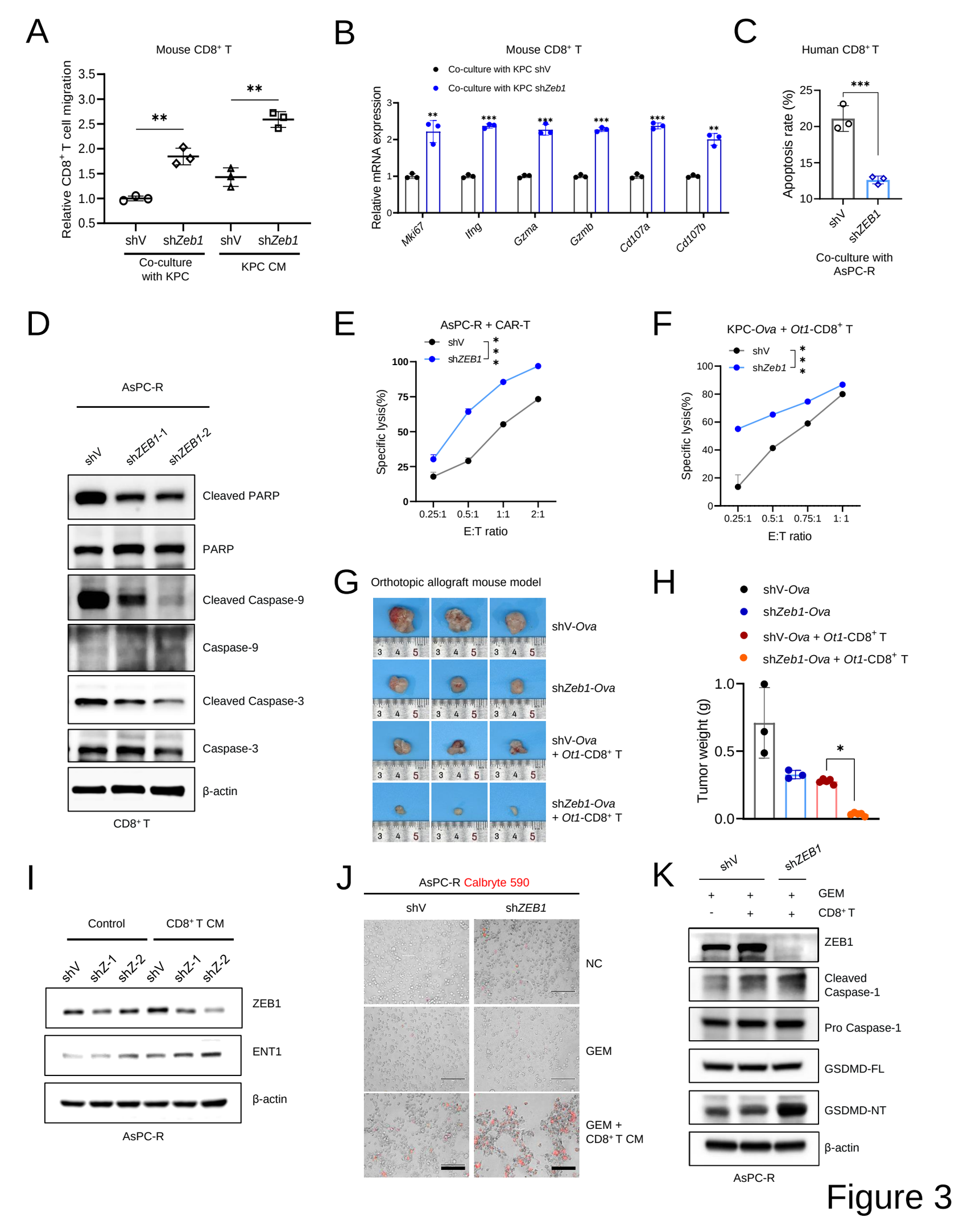
A
Mouse CD8⁺ T
Relative CD8⁺ T cell migration
shV
shZeb1
shV
shZeb1
Co-culture with KPC
KPC CM
B
Mouse CD8⁺ T
Co-culture with KPC shV
Co-culture with KPC shZeb1
Relative mRNA expression
Mki67
Ifng
Gzma
Gzmb
Cd107a
Cd107b
C
Human CD8⁺ T
Apoptosis rate (%)
shV
shZEB1
Co-culture with AsPC-R
D
AsPC-R
shV
shZEB1-1
shZEB1-2
Cleaved PARP
PARP
Cleaved Caspase-9
Caspase-9
Cleaved Caspase-3
Caspase-3
β-actin
CD8⁺ T
E
AsPC-R + CAR-T
shV
shZEB1
Specific lysis(%)
E:T ratio
F
KPC-Ova + Ot1-CD8⁺ T
shV
shZeb1
Specific lysis(%)
E:T ratio
G
Orthotopic allograft mouse model
shV-Ova
shZeb1-Ova
shV-Ova + Ot1-CD8⁺ T
shZeb1-Ova + Ot1-CD8⁺ T
H
shV-Ova
shZeb1-Ova
shV-Ova + Ot1-CD8⁺ T
shZeb1-Ova + Ot1-CD8⁺ T
Tumor weight (g)
I
Control
CD8⁺ T CM
shV
shZ-1
shZ-2
shV
shZ-1
shZ-2
ZEB1
ENT1
β-actin
AsPC-R
J
AsPC-R Calbryte 590
shV
shZEB1
NC
GEM
GEM + CD8⁺ T CM
K
shV
shZEB1
GEM
CD8⁺ T
ZEB1
Cleaved Caspase-1
Pro Caspase-1
GSDMD-FL
GSDMD-NT
β-actin
AsPC-R

Figure 3

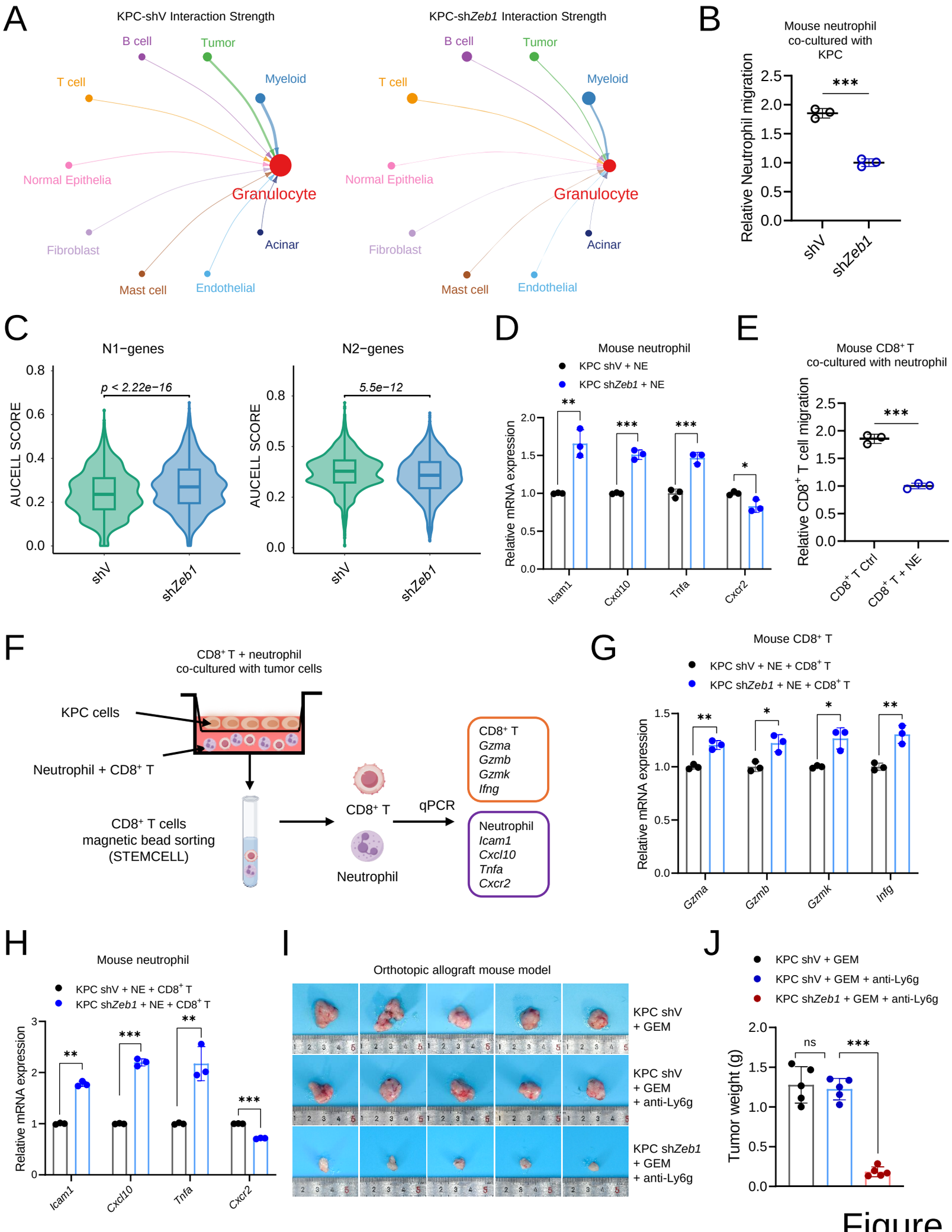
A
KPC-shV Interaction Strength
KPC-shZeb1 Interaction Strength
B cell
Tumor
T cell
Myeloid
Normal Epithelia
Granulocyte
Fibroblast
Acinar
Mast cell
Endothelial
B
Mouse neutrophil co-cultured with KPC
Relative Neutrophil migration
***
shV
shZeb1
C
N1−genes
N2−genes
p < 2.22e−16
5.5e−12
AUCELL SCORE
shV
shZeb1
D
Mouse neutrophil
KPC shV + NE
KPC shZeb1 + NE
Relative mRNA expression
Icam1
Cxcl10
Tnfa
Cxcr2
E
Mouse CD8+ T co-cultured with neutrophil
Relative CD8+ T cell migration
CD8+ T Ctrl
CD8+ T + NE
F
CD8+ T + neutrophil co-cultured with tumor cells
KPC cells
Neutrophil + CD8+ T
CD8+ T cells magnetic bead sorting (STEMCELL)
CD8+ T
Neutrophil
qPCR
CD8+ T
Gzma
Gzmb
Gzmk
Ifng
Neutrophil
Icam1
Cxcl10
Tnfa
Cxcr2
G
Mouse CD8+ T
KPC shV + NE + CD8+ T
KPC shZeb1 + NE + CD8+ T
Relative mRNA expression
Gzma
Gzmb
Gzmk
Ifng
H
Mouse neutrophil
KPC shV + NE + CD8+ T
KPC shZeb1 + NE + CD8+ T
Relative mRNA expression
Icam1
Cxcl10
Tnfa
Cxcr2
I
Orthotopic allograft mouse model
KPC shV + GEM
KPC shV + GEM + anti-Ly6g
KPC shZeb1 + GEM + anti-Ly6g
J
KPC shV + GEM
KPC shV + GEM + anti-Ly6g
KPC shZeb1 + GEM + anti-Ly6g
Tumor weight (g)
ns
***

Figure 4

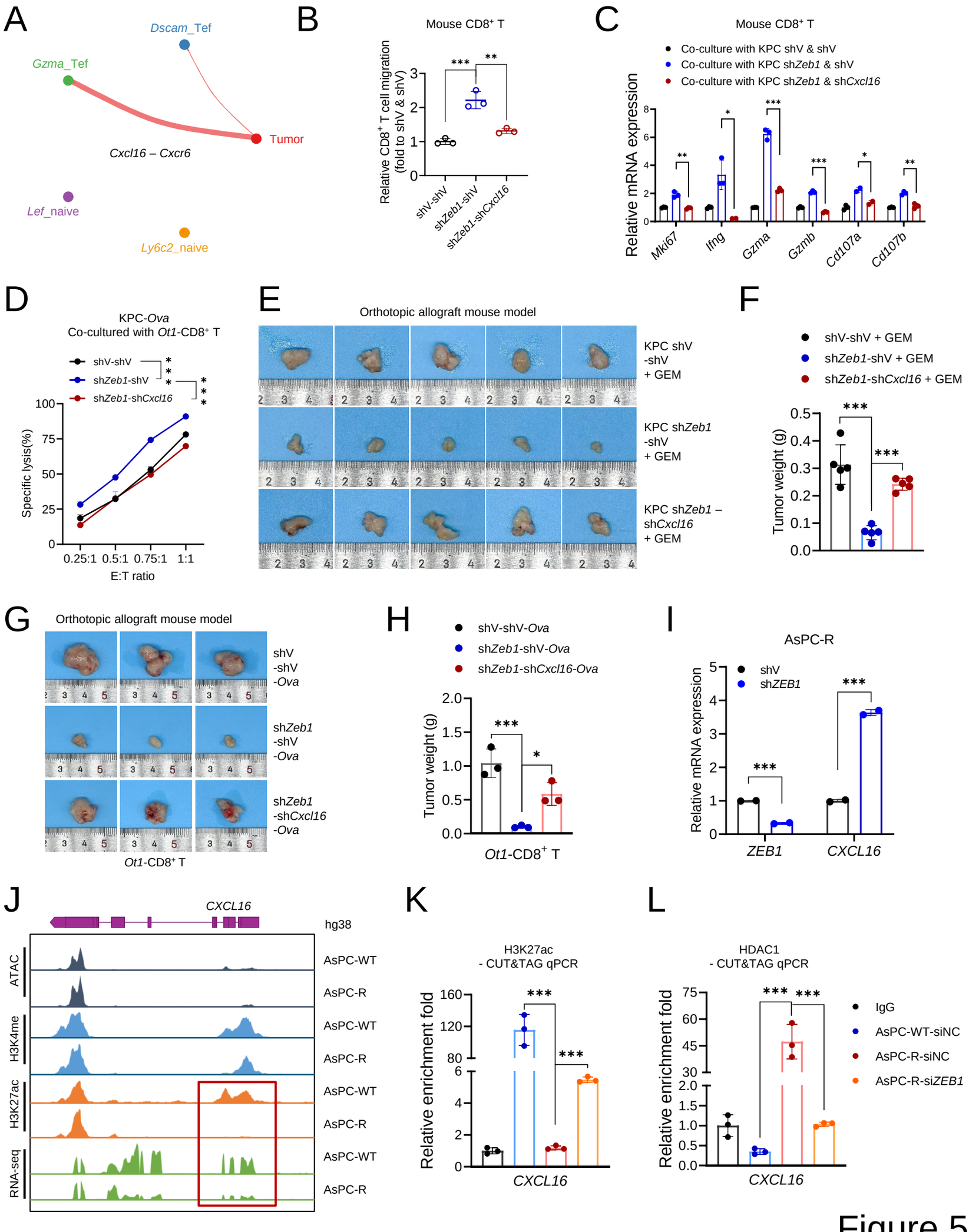
A
Dscam_Tef
Gzma_Tef
Tumor
Cxcl16 – Cxcr6
Lef_naive
Ly6c2_naive
B
Mouse CD8+ T
Relative CD8+ T cell migration (fold to shV & shV)
shV-shV
shZeb1-shV
shZeb1-shCxcl16
C
Mouse CD8+ T
Co-culture with KPC shV & shV
Co-culture with KPC shZeb1 & shV
Co-culture with KPC shZeb1 & shCxcl16
Relative mRNA expression
Mki67
Ifng
Gzma
Gzmb
Cd107a
Cd107b
D
KPC-Ova
Co-cultured with Ot1-CD8+ T
shV-shV
shZeb1-shV
shZeb1-shCxcl16
Specific lysis(%)
E:T ratio
E
Orthotopic allograft mouse model
KPC shV -shV + GEM
KPC shZeb1 -shV + GEM
KPC shZeb1 – shCxcl16 + GEM
F
shV-shV + GEM
shZeb1-shV + GEM
shZeb1-shCxcl16 + GEM
Tumor weight (g)
G
Orthotopic allograft mouse model
shV -shV -Ova
shZeb1 -shV -Ova
shZeb1 -shCxcl16 -Ova
Ot1-CD8+ T
H
shV-shV-Ova
shZeb1-shV-Ova
shZeb1-shCxcl16-Ova
Tumor weight (g)
Ot1-CD8+ T
I
AsPC-R
shV
shZEB1
Relative mRNA expression
ZEB1
CXCL16
J
CXCL16
hg38
ATAC
H3K4me
H3K27ac
RNA-seq
AsPC-WT
AsPC-R
K
H3K27ac
- CUT&TAG qPCR
Relative enrichment fold
CXCL16
L
HDAC1
- CUT&TAG qPCR
IgG
AsPC-WT-siNC
AsPC-R-siNC
AsPC-R-siZEB1
Relative enrichment fold
CXCL16

Figure 5

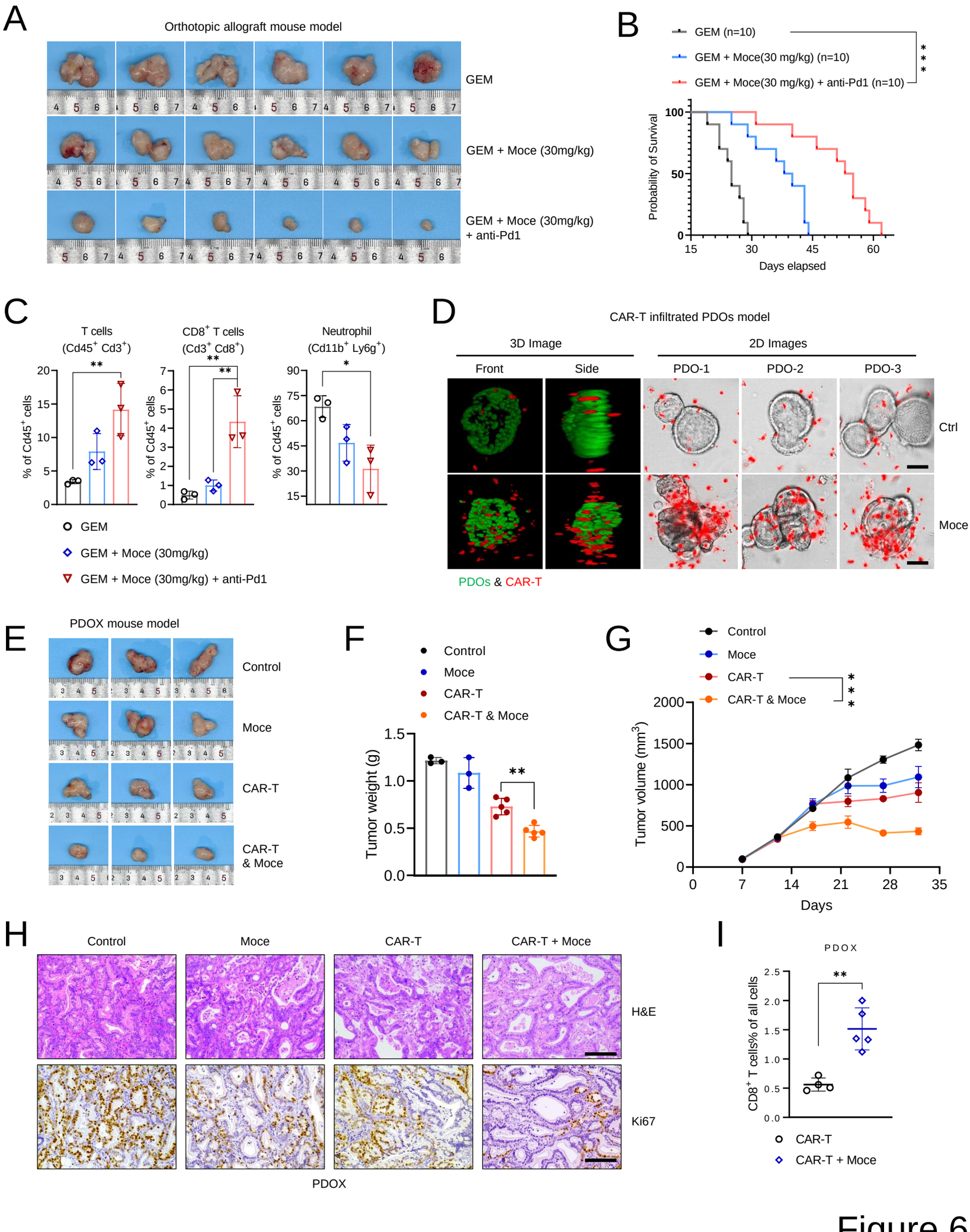
A
Orthotopic allograft mouse model
GEM
GEM + Moce (30mg/kg)
GEM + Moce (30mg/kg)
+ anti-Pd1
B
GEM (n=10)
GEM + Moce(30 mg/kg) (n=10)
GEM + Moce(30 mg/kg) + anti-Pd1 (n=10)
***
Probability of Survival
100
50
0
15
30
45
60
Days elapsed
C
T cells
(Cd45+ Cd3+)
CD8+ T cells
(Cd3+ Cd8+)
Neutrophil
(Cd11b+ Ly6g+)
% of Cd45+ cells
**
**
**
*
GEM
GEM + Moce (30mg/kg)
GEM + Moce (30mg/kg) + anti-Pd1
D
CAR-T infiltrated PDOs model
3D Image
2D Images
Front
Side
PDO-1
PDO-2
PDO-3
Ctrl
Moce
PDOs & CAR-T
E
PDOX mouse model
Control
Moce
CAR-T
CAR-T
& Moce
F
Control
Moce
CAR-T
CAR-T & Moce
Tumor weight (g)
**
G
Control
Moce
CAR-T
CAR-T & Moce
***
Tumor volume (mm3)
Days
H
Control
Moce
CAR-T
CAR-T + Moce
H&E
Ki67
PDOX
I
PDOX
CD8+ T cells% of all cells
**
CAR-T
CAR-T + Moce

Figure 6

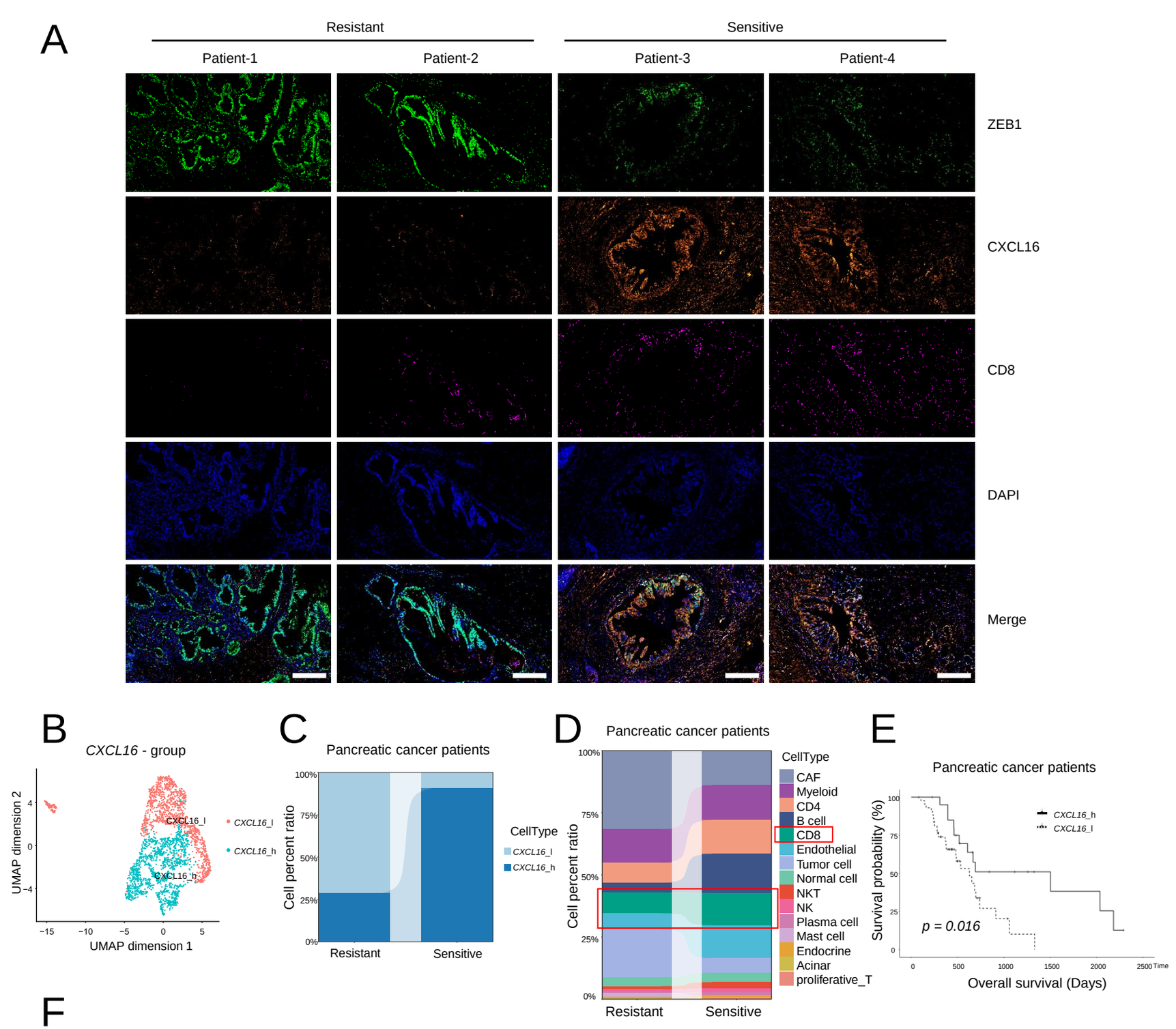
A
Resistant
Sensitive
Patient-1
Patient-2
Patient-3
Patient-4
ZEB1
CXCL16
CD8
DAPI
Merge
B
CXCL16 - group
UMAP dimension 2
UMAP dimension 1
CXCL16_l
CXCL16_h
C
Pancreatic cancer patients
Cell percent ratio
Resistant
Sensitive
CellType
CXCL16_l
CXCL16_h
D
Pancreatic cancer patients
Cell percent ratio
CellType
CAF
Myeloid
CD4
B cell
CD8
Endothelial
Tumor cell
Normal cell
NKT
NK
Plasma cell
Mast cell
Endocrine
Acinar
proliferative_T
E
Pancreatic cancer patients
Survival probability (%)
p = 0.016
Overall survival (Days)
F
Immune suppressive TME and GEM resistance
Gemcitabine
PDAC cell
Neutrophil
CD44
ENT1
SPP1
GEM↓ transportation
HDAC1
ZEB1
reduced acetylation
H3K27
CXCL16
PD-L1
PD-1
CD8⁺T
• Decreased CD8⁺ T cell recruitment
• Inhibited CD8⁺ T cell cytotoxic effect
Active T cell response and GEM sensitivity
Gemcitabine
PDAC cell
Neutrophil
CD44
ENT1↑
SPP1↓
GEM transportation ↑
Pyroptosis ↑
HDAC1
ZEB1↓
HDAC inhibitors
H3K27
CXCL16↑
MHC I↑
TCR
GZMA⁺CD8⁺T
PD-1
PD-L1
CXCR6
CXCL16
• Increased CD8⁺ T cell recruitment
• Enhanced CD8⁺ T cell cytotoxic effect

Figure 7